Res. Rep. Fac. Eng. Mie. Univ., Vol.32,pp. 1-23(2007)
Original Paper

Ferromagnetism and Superconductivity in Two-band Hubbard Models

Kazuhiro Sano and Yoshiaki Ōno*
(Department of Physics Engineering)

(Received July 18, 2007)

Abstract

We investigate ferromagnetism and superconductivity in two types of two-band Hubbard models: the multi-orbital Hubbard model and the *d-p* model, with particularly paying attention to effect of the interplay between the electron correlation and the band splitting. As strong correlation plays a crucial role for these phenomena, we employ two complementary approaches: the numerical diagonalization method for one-dimensional models and the dynamical mean-field theory for the infinite-dimensional model. These approaches give us reliable results beyond the perturbative approximation or the usual mean-field like approximation. For the one-dimensional models, we calculate the critical exponent K_ρ based on the Tomonaga-Luttinger liquid theory and determine phase diagram of superconducting(SC) region by the condition $K_\rho > 1$. The SC region appears near partially polarized ferromagnetic region in the multi-orbital Hubbard model with finite band splitting. Analysis of paring correlation functions for the ground state indicates that the triplet paring is relevant to the superconductivity. In the one-dimensional *d-p* model, we find enhancements of the singlet and triplet paring correlations at the SC region. Although only the singlet paring is relevant to superconductivity near half-filling, the triplet paring increases with electron filling and is relevant to the superconductivity as well as the singlet paring near full-filling. In the infinite-dimensional *d-p* model, we calculate the local green's function on the basis of the dynamical mean-field theory, where the effective impurity Anderson model is solved using the numerical diagonalization method. It shows the phase diagrams of the metal-insulator transition on the ground state at half-filling and quarter-filling as functions of the Coulomb interaction and the band splitting. We obtain the transition temperatures for the ferromagnetism and the superconductivity as functions of the Coulomb interaction, the band splitting and the electron filling. It indicates that the transition temperature of the triplet superconductivity is higher than that of the singlet superconductivity near the ferromagnetic state. These results suggest a close relationship between the ferromagnetism and the superconductivity as a common feature of the two-band Hubbard models.

1 Introduction

The strongly correlated electron systems with multi-band (multi-orbital) have attracted much interest due to various interesting phenomena such as colossal magnetoresistance in manganites $La_{1-x}Sr_xMnO_3$[1], triplet-pairing superconductivity in the ruthenate Sr_2RuO_4[2], metal-insulator transition in alkali-doped fullerides A_xC_{60}[3] and one-dimensional superconductivity of CuO_2 double chain in $Pr_2Ba_4Cu_7O_{15-\delta}$[4]. Among them, spin-state transition of cobalt oxides in $La_{1-x}Sr_xCoO_3$[5, 6, 7] give a good example displaying the effect of multi-orbital. Since the Hund's rule coupling and the crystal-field splitting between the t_{2g} and e_g orbitals are close to each other, the spin state of the cobalt ion depends on temperature, doping concentration and crystal structure. With increasing temperature, the low-spin state ($t_{2g}^6e_g^0$, $S = 0$) of the Co^{3+} ($3d^6$) ion gradually changes into an intermediate-spin state ($t_{2g}^5e_g^1$, $S = 1$) and/or a high-spin (HS) state ($t_{2g}^4e_g^2$, $S = 2$)[6, 7, 8, 9]. With Sr doping, $La_{1-x}Sr_xCoO_3$ shows a spin-glass state for $x < 0.18$ and a ferromagnetism for $x > 0.18$[10, 11].

Layered cobalt oxides such as Na_xCoO_2 also show a a variety of interesting properties as multi-band systems. For example, large thermoelectric power is discovered in $Na_{0.5}CoO_2$[12]. Weak ferromagnetism has been observed in $Na_{0.75}CoO_2$[13]. The discovery of the superconductivity[14] in $Na_xCoO_2 \cdot yH_2O$ with $T_c \approx 5K$ for $x \approx 0.35$ and $y \approx 1.3$ has stimulated considerable attention on these materials. It has been suggest that large degeneracy of electronic states due to a competition

*Department of Physics, Niigata University

between the Hund's rule coupling and the crystal-field splitting plays a key role in the electronic states of Na_xCoO_2 as well as of $La_{1-x}Sr_xCoO_3$[15].

With the new findings of these interesting materials, theoretical studies on the interplay between Coulomb interactions including the Hund's rule coupling and band splitting by crystal-field are highly desirable. The orbitally degenerate Hubbard model, which can be regarded as a kind of multi-band system, has been extensively investigated to clarify the effect of orbital degrees of freedom in the presence of intra-atomic Coulomb interaction. Many authors[16, 17, 18, 19, 20, 21, 22, 23, 24, 25, 26] have studied the ferromagnetism of this model and revealed that Hund's rule coupling plays a crucial role in ferromagnetism.

On the other hand, multi-band Hubbard model, which includes the effect of band splitting explicitly, has also been extensively studied for a long time. In particular, there has been much theoretical interest in the *d*-*p* model as a model of the copper oxide high-temperature superconductor. The model contains hopping t_{pd} between the Cu (*d*-orbital) site and the O(*p*-orbital) site and strong repulsive interactions at the *d* and *p* site (U_d and U_p, respectively). In addition, it can contain the nearest-neighbor *d*-*p* interaction U_{pd} and/or hopping t_{pp} between the nearest-neighbor *p* sites. It is widely accepted as a basic model describing the electronic structure of the Cu-O network. Many theoretical studies have been performed on this model to explain the superconductivity and/or the antiferromagnetism of the copper oxides. A few work has been discussed the possibility of so called flat band ferromagnetism in a type of *d*-*p* model[27].

In the present work, we address the multi-orbital Hubbard model in one-dimension and the *d*-*p* model in one- and infinite-dimension, while particularly paying attention to the effect of the interplay between the Coulomb interactions and the band splitting Δ. At the point of view of ferromagnetism and superconductivity in itinerant electron systems, we discuss these two models in detail. As the strong correlation effect plays crucial roles in these interesting phenomena, a nonperturbative and reliable approach is required. We employ the numerical diagonalization method for the multi-orbital Hubbard model and the *d*-*p* model with finite system sizes in one-dimension, and the dynamical mean field theory for the infinite-dimensional *d*-*p* model. These approaches are complementary for each other in dimensionality and expected to give us reliable results beyond the perturbative or the mean-field like approximations.

Numerical diagonalization approach has already been applied for the multi-orbital Hubbard model at $\Delta = 0$ case[17, 18]. Although the available system size is fairly small, the results are in good agreement with the strong coupling analysis[18] and the results from the density-matrix renormalization-group method[23]. To examine the superconductivity, we calculate the critical exponent of the correlation functions K_ρ based on the Luttinger liquid theory[28, 29, 30, 31]. The reliability of this approach has been extensively tested for various one-dimensional models such as the Hubbard model[32], the *t*-*J* model[33] and the *U*-*V* model[34]. We can thus expect that this approach is reliable for the multi-orbital Hubbard model and the *d*-*p* model as well.

In the limit of infinite dimensions, the self-energy becomes purely site-diagonal and the dynamical mean field theory (DMFT) becomes exact. The local Green's function is given by the impurity Green's function of an effective single impurity Anderson model. This effective one-site problem is calculated by the numerical diagonalization of the finite size clusters. By using this method, Momoi et al. studied the multi-orbital Hubbard model at $\Delta = 0$[17]. They show the phase diagram of the ferromagnetism, but superconductivity was not discussed there. By calculating the magnetization and the pairing susceptibility at finite temperature, we show the transition temperatures for the ferromagnetism and the superconductivity as functions of the Coulomb interaction, the band splitting and the electron filling.

2 Luttinger Liquid Relation

At first, we briefly discuss a general argument for 1D-electron systems based on the Luttinger liquid theory. In the Luttinger liquid theory[28, 29, 30, 31], an effective Hamiltonian of 1D models in the Tomonaga-Luttinger regime is generally given by

$$H = \frac{v_\sigma}{2\pi}\int_0^L \mathrm{d}x \left[K_\sigma(\partial_x\theta_\sigma)^2 + K_\sigma^{-1}(\partial_x\phi_\sigma)^2\right] + \frac{v_\rho}{2\pi}\int_0^L \mathrm{d}x \left[K_\rho(\partial_x\theta_\rho)^2 + K_\rho^{-1}(\partial_x\phi_\rho)^2\right], \tag{1}$$

where v_σ, v_ρ, K_σ and K_ρ are the velocities and coupling parameters of spin and charge parts, respectively. According to the Luttinger liquid theory, some relations have been established as universal

relations in one-dimensional single band models[30, 31]. In the model which is isotropic in spin space, the coupling constant K_σ is renormalized to unity in the low energy limit and the critical exponents of various types of correlation functions are determined by a single parameter K_ρ.

For single band model, it is predicted that SC correlation is dominant for $K_\rho > 1$ (the correlation function decays as $\sim r^{-(1+\frac{1}{K_\rho})}$ in the Tomonaga-Luttinger (TL) regime and as $\sim r^{-\frac{1}{K_\rho}}$ in the Luther-Emery (LE) regime), whereas the CDW or SDW correlations are dominant for $K_\rho < 1$ (the correlation functions decay as $\sim r^{-(1+K_\rho)}$ in the TL regime and as $\sim r^{-K_\rho}$ in the LE regime). Here, the LE regime is characterized by a gap in the spin excitation spectrum, while in the TL regime, the excitation is gapless[28, 31]. In the case of non-interacting fermion systems, the exponent K_ρ is always unity. Thus, the effective interaction between quasi-particles is attractive for $K_\rho > 1$ whereas that is repulsive for $K_\rho < 1$.

The critical exponent K_ρ is related to the charge susceptibility χ_c and the Drude weight D by

$$K_\rho = \frac{1}{2}(\pi\chi_c D)^{1/2}, \tag{2}$$

with $D = \frac{\pi}{N_u}\frac{\partial^2 E_0(\phi)}{\partial\phi^2}$, where $E_0(\phi)$ is the total energy of the ground state as a function of magnetic flux $N_u\phi$[31]. Here, the flux is imposed by introducing the following gauge transformation: $c_{m\sigma}\dagger \rightarrow e^{im\phi/N_a}c^\dagger_{m\sigma}$ for an arbitrary site m. When the charge gap vanishes in the thermodynamic limit, the uniform charge susceptibility χ_c is obtained from

$$\chi_c = \frac{4/N_u}{E_0(N_e+2,N_u)+E_0(N_e-2,N_u)-2E_0(N_e,N_u)}, \tag{3}$$

where $E_0(N_e, N_u)$ is the ground state energy of a system with N_u unit sites(cells) and N_e electrons. The filling n is defined by $n = N_e/N_u$, where N_u is the total number of unit cells or sites. The values of D and χ_c are calculated from the ground state energy of the finite size system through eq.(2) and (3).

It is noted that the situation is complicated for two-band models. When both bands have been occupied by electrons simultaneously, Fermi points appear in both bands. In this case, the electronic state of the low energy is completely changed and we can not use the above relations[35, 36, 37, 38]. On the other hand, if the electron density is sufficiently small and/or the band splitting is sufficiently large, electrons occupy only lower band. In this case, Fermi level exits in only lower band and the low energy effective Hamiltonian is considered to be equivalent to that of the single band model. Therefore, we can adopt the above Luttinger liquid relations of the single band model for even two-band model.

We numerically diagonalize the model Hamiltonian and obtain the value of K_ρ from the ground state energy of finite size systems using the standard Lanczos algorithm. In addition to the numerical diagonalization method, we use mean-field(MF) approximation to calculate the ground state energy and obtain the approximate value of K_ρ of the infinite system. This approximation has been confirmed to be reliable at least in the weak coupling regime[39].

3 Multi-orbital Hubbard Model

Previous works[17, 18, 19, 20, 21, 22, 23, 24] have studied the multi-orbital Hubbard model in the case of the crystal-field splitting $\Delta = 0$. In one dimension, some rigorous results are shown in the strong coupling limit $U \rightarrow \infty$: the ground state is a fully polarized ferromagnetism for $0 < n < 2$ except for $n = 1$ when U' and $J = J'$ are positive and finite[21]. The numerical result suggests that the ferromagnetism is stable also for $n = 1$ in the strong coupling region[23]. In infinite dimensions, the dynamical mean-field theory shows the existence of the ferromagnetism in the same parameter region observed in one dimension[22]. They revealed that Hund's rule coupling J plays a crucial role in ferromagnetism. However, possible mechanisms of superconductivity and the effect of crystal-field splitting Δ was not considered in these studies.

In this section, we examine ferromagnetism and related superconductivity in the multi-orbital Hubbard model, while particularly paying attention to the effect of the interplay between J and Δ[40, 41, 42].

3.1 Model Hamiltonian

We consider the following Hamiltonian for the one-dimensional multi-orbital Hubbard model:

$$\begin{aligned} H &= -t\sum_{i,m,\sigma}(c^{\dagger}_{i,m,\sigma}c_{i+1,m,\sigma}+h.c.)+U\sum_{i,m}n_{i,m,\uparrow}n_{i,m,\downarrow} \\ &+ U'\sum_{i,\sigma}n_{i,u,\sigma}n_{i,l,-\sigma}+(U'-J)\sum_{i,\sigma}n_{i,u,\sigma}n_{i,l,\sigma}+\frac{\Delta}{2}\sum_{i,\sigma}(n_{i,u,\sigma}-n_{i,l,\sigma}) \\ &- J\sum_{i,m}(c^{\dagger}_{i,u,\uparrow}c_{i,u,\downarrow}c^{\dagger}_{i,l,\downarrow}c_{i,l,\uparrow}+h.c.)-J'\sum_{i,m}(c^{\dagger}_{i,u,\uparrow}c^{\dagger}_{i,u,\downarrow}c_{i,l,\uparrow}c_{i,l,\downarrow}+h.c.), \end{aligned} \tag{4}$$

where $c^{\dagger}_{i,m,\sigma}$ stands for the creation operator of an electron with spin σ in the orbital m $(=u,l)$ at site i and $n_{i,m,\sigma}=c^{\dagger}_{i,m,\sigma}c_{i,m,\sigma}$. Here, t represents the hopping integral between the same orbitals and we set $t=1$ in this study.

The interaction parameters U, U', J and J' stand for the intra- and inter-orbital direct Coulomb interactions, the exchange (Hund's rule) coupling and the pair-transfer, respectively. Δ denotes the energy difference between the two atomic orbitals, that is, crystal-field splitting. For simplicity, we impose the relations, $J=J'$ and $U=U'+2J$; the latter holds exactly in $3d$-orbitals for $\Delta=0$ and is a good approximation for $\Delta\neq 0$. The model in eq. (4) is schematically represented by Fig. 1(a). We numerically diagonalize the above model Hamiltonian up to 9 sites. In the noninteracting case $(U=U'=J=0)$, the Hamiltonian eq. 4 yields a dispersion relation $\epsilon^{\pm}(k)=-2t\cos(k)\pm\frac{\Delta}{2}$, where k is the wave vector and $\epsilon^{+}(k)$ $(\epsilon^{-}(k))$ represents the upper (lower) band energy. This band structure is schematically represented by Fig. 1(b).

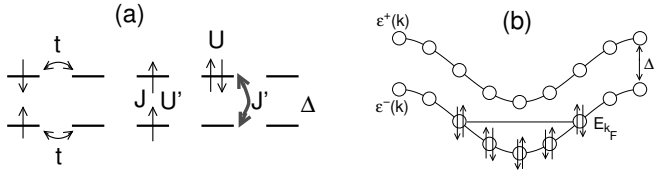

Figure 1: Schematic diagrams of (a) the model Hamiltonian and (b) the band structure in the noninteracting case.

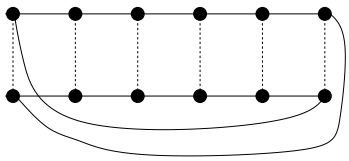

Figure 2: Schematic diagram of Moebius boundary condition at $\Delta=0$.

3.2 Result for degenerate case

We first exhibit the result at $\Delta=0$ and compare it with the previous works. At $\Delta=0$, two bands are doubly degenerate and the finite size effect of the ordinary periodic boundary condition is fairly large. To reduce it, we use the Moebius boundary condition, which has been already used in t-J ladder models[43]. The Moebius boundary condition as shown in Fig.2, is a kind of the periodic boundary condition and efficiently reduces the finite size effect of the systems than the ordinary periodic boundary condition.

Figure 4 shows the phase diagram of the ground state for the $N_u=8$ system at $n=0.5$ (4electrons/8sites) with the result of the DMRG method by Sakamoto et al.[23] on the U' vs. J parameter plane. A ferromagnetic ground state with full spin polarization($S=max$) appears around $J\simeq U'$ for $U'\gtrsim 3$. The parameter regions $J/U'\gg 1$ and $J/U'\ll 1$ are paramagnetic($S=0$). No partially polarized state was found at this filling. Figure also shows that the difference between our result and the DMRG result is small. The present result is similar to those by previous studies employing the periodic or the anti-periodic boundary conditions, but the phase boundaries of their ferromagnetic phases seem to depend on the system size greatly. We also indicate the phase boundary of the ferromagnetic phase by using the mean-field(MF) approximation in Fig.4. In this approximation, the ground-state energy E_0 is calculated as

$$\begin{aligned} E_0 &= <H> \\ &= \sum_{k<k_F,m,\sigma}\epsilon^{\pm}(k)+UN_u\sum_{m}<n_{m,\uparrow}><n_{m,\downarrow}>+U'N_u\sum_{\sigma}<n_{u,\sigma}><n_{l,-\sigma}> \\ &+ (U'-J)N_u\sum_{\sigma}<n_{u,\sigma}><n_{l,\sigma}>+\frac{\Delta}{2}N_u\sum_{\sigma}(<n_{u,\sigma}>-<n_{l,\sigma}>), \end{aligned} \tag{5}$$

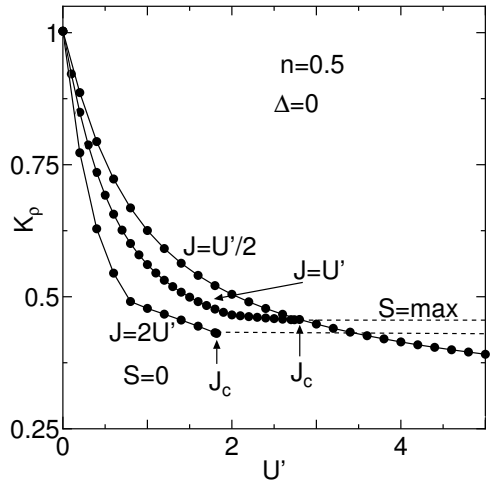

Figure 3: K_ρ as a function of U' in the cases of $J = U'/2$, $J = U'$ and $J = 2U'$ at $n = 0.5(4electrons/8sites)$. J_c indicates the critical point of the singlet ground state changing into the fully polarized ferromagnetic(S=max) ground state.

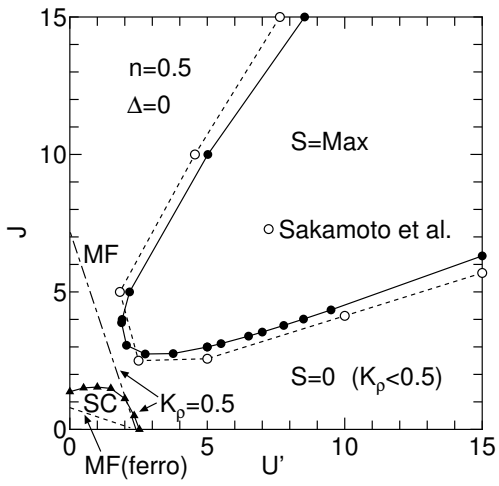

Figure 4: Phase diagram of the ferromagnetic state on the $U'-J$ parameter plane for $n = 0.5$(4electrons/8sites) at $\Delta = 0$. The dashed line represents the phase boundary of the ferromagnetic state obtained by MF approximation. The solid triangle shows the point of $K_\rho = 0.5$ on the U'-axis.

where <> represents the expectation value of operators by the noninteracting ground state. Here, the terms $-J\sum_{i,m}(c^\dagger_{i,u,\uparrow}c_{i,u,\downarrow}c^\dagger_{i,l,\downarrow}c_{i,l,\uparrow} + h.c.)$ and $-J'\sum_{i,m}(c^\dagger_{i,u,\uparrow}c^\dagger_{i,u,\downarrow}c_{i,l,\uparrow}c_{i,l,\downarrow} + h.c.)$ are omitted since the expectation values of these terms are equal to zero. The result indicates that the ferromagnetic phase appears all over the region except the near the origin. Comparing with the numerical results, it seems to overestimate the ferromagnetic region.

Figure 5 shows the value of K_ρ as a function of U' for $J = 0$ at quarter filling $n = 1$(4electrons/4sites). We also show the result of the Green's function Monte Carlo method obtained by Assaraf et al.[44] and the MF approximation for K_ρ[39], which are represented by the broken and the dashed lines in fig.5, respectively. Here, K_ρ of the MF approximation is estimated by the Luttinger liquid relation as well as Numerical diagonalization method and the ground state is restricted to the singlet state, that is, the condition $< n_{m,\uparrow} >=< n_{m,\downarrow} >$ is imposed. It shows good agreement with the numerical result in the weak coupling regime, ensuring the small finite-size effect of the numerical calculation. As U' increases, K_ρ decreases from unity to ~ 0.42. For $J = 0$, the model Hamiltonian is equivalent to the SU(4) Hubbard model and the metal-insulator(MI) transition occurs at $K_\rho = 0.5$[44]. When U' is larger than a critical value $U'_c \sim 3$, the MI transition is expected. Sakamoto et al. show the n-dependence of the chemical potential at quarter filling and the existence of large charge gap in the strong coupling region. Although the finite size effect does not allow the correct estimation of the transition point, they claim that the metal-insulator transition occurs at finite positive value of $U' = J \sim 3$.

Figure 6 gives the value of K_ρ as a function of U' in several conditions of $J = U'/2$, $J = U'$ and $J = 2U'$ at $n = 1$. As U' increases, K_ρ decreases, while it increases for a large U' in the condition $J = 2U'$. In the region $K_\rho > 0.5$, the SC correlation is expected to be the most dominant compared with the CDW and SDW correlations. To confirm the SC state, we calculate the lowest energy of the singlet state $E_0(\phi)$ as a function of an external flux ϕ. As shown in Fig.7, the anomalous flux quantization occurs in the region $K_\rho > 0.5$, where the signature of it increases with J. It indicates that the SC state is surely realized in this parameter region.

In Figure 8, we give the phase diagram of the ground state for $N_u = 4$ at the electron density $n = 1$(4electrons/4sites) with the result of DMRG method[23] on the U' vs. J parameter plane. A complete ferromagnetism with S=max appears around $J \simeq U'$ in the strong coupling regime. This result is in good agreement with the DMRG result obtained by Sakamoto *et al.*[23]. The dashed line presents the boundary between the ferromagnetic state and the singlet state by using the mean-field approximation. It seems to be fairly overestimate for the ferromagnetic region. It also indicates that

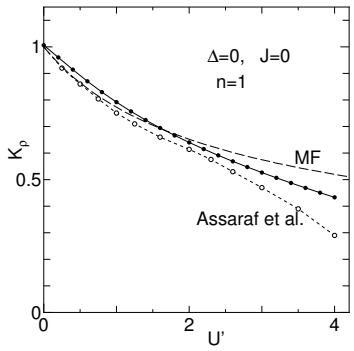

Figure 5: K_ρ as a function of U' in the cases of $J = 0$ for $n = 1.0$ (4electrons/4sites) at $\Delta = 0$. The dashed line represents a MF estimation for K_ρ. The broken line indicates the GFMC result obtained by Assaraf et al.

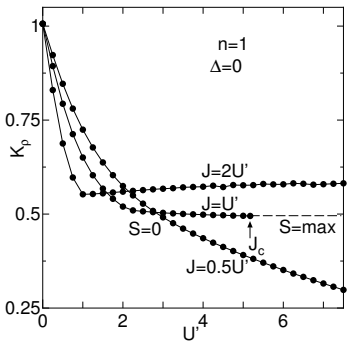

Figure 6: K_ρ as a function of U' in the cases of $J = U'/2$, $J = U'$ and $J = 2U'$ for $n = 1.0$ (4electrons/4sites) at $\Delta = 0$.

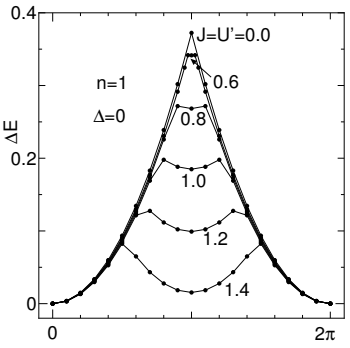

Figure 7: The energy difference $E_0(\phi) - E_0(0)$ as a function of an external flux ϕ at $n = 1.0$(6electrons/6sites) at $\Delta = 0$.

the ferromagnetic region is smaller than the case of $n = 0.5$. In this ferromagnetic region, Sakamoto *et al.* also claimed that the system shows the triplet SC for $J > U'$, while it becomes insulator for $J < U'$. The SC phase boundary in the ferromagnetic region is smoothly connected to that in the paramagnetic region as shown in Fig. 8. These results tell us that the Hund's rule coupling J plays important roles not only for the ferromagnetism but also for the superconductivity. In the paramagnetic state (S=0), we plot the phase boundary separating the SC region with $K_\rho > 0.5$ and the insulating region with $K_\rho < 0.5$. As mentioned above, this SC phase is confirmed by the anomalous flux quantization, while this quantization disappears in the insulating region with large U' (not shown). Within the bosonaization method, the SC state has been identified as the triplet SC with spin gap[25]. However, very recent work claims that the relevant symmetry of the paring is not

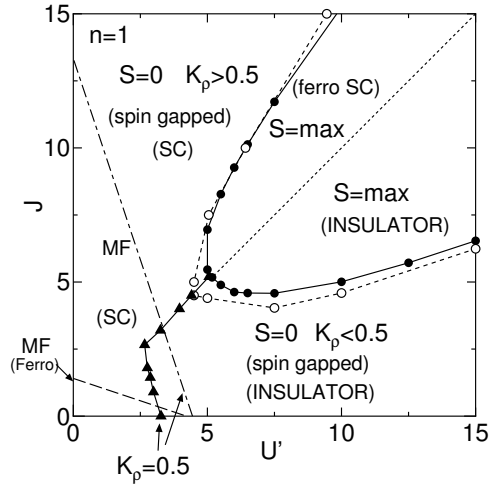

Figure 8: Phase diagram of the ferromagnetic state on the $U' - J$ parameter plane for $n = 1$(4electrons/4sites) at $\Delta = 0$. The dashed line represents the phase boundary of the ferromagnetic state obtained by MF approximation. The solid triangle shows the point of $K_\rho = 0.5$ on the U'-axis.

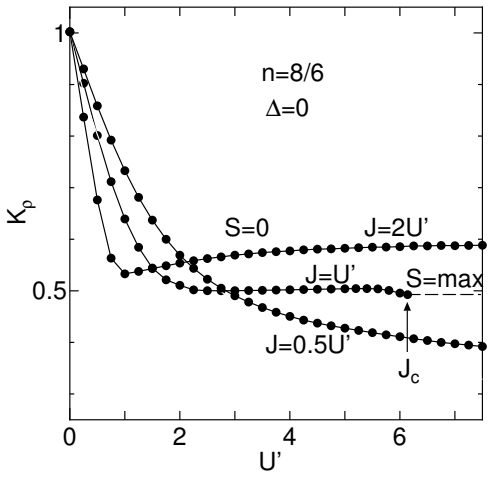

Figure 9: K_ρ as a function of U' for $n = 4/3$ (8electrons/6sites) at $\Delta = 0$.

$'p-'$ wave like triplet but $'d_{xy}-'$ like singlet by using the bosonaization method and DMRG method within the model at $U'=0$[26].

To examine the case of over the quarter-filling(n=1), we calculate the value of K_ρ as a function of U' in several conditions of $J=U'/2$, $J=U'$ and $J=2U'$ at $n=4/3$ (8electrons/6sites). As shown in Figure 9, it seems to be similar to the case of ($n \leq 1$. This result suggests that the overall aspect of the electronic state dose not much depend on n.

3.3 Case for finite Δ

Next, we consider the case of $\Delta > 0$. When the lowest energy of the upper band, $\epsilon^+(0)$, is larger than the Fermi energy, E_{k_F}, electrons occupy only the lower band with $k_F = \frac{\pi n}{2}$ and the model is regarded as a "single component" electron system. Hereafter, we mainly treat the case with $\epsilon^+(0) > E_{k_F}$. In this case, we can not adopt the Moebius boundary condition, since the symmetry of inter-band is broken by finite Δ. In the case $n < 1$, we find the following boundary conditions are suitable, that is, the periodic(antiperiodic) boundary condition for the lower(upper) band at $N_e = 4m+2$ and the antiperiodic(periodic) boundary condition for the upper(lower) band at $N_e = 4m$, where N_e is the total electron number and m is an integer. This boundary condition can be regard as an extension of the Moebius boundary condition for the finite Δ.

For $n > 1$, on the other hand, our experience indicates that the usual boundary conditions, that is, the periodic boundary condition at $N_e = 4m+2$ and the antiperiodic boundary condition at $N_e = 4m$ for the both bands, are little better. This choice of the boundary conditions is rather empirical, but it seems to lead better results.

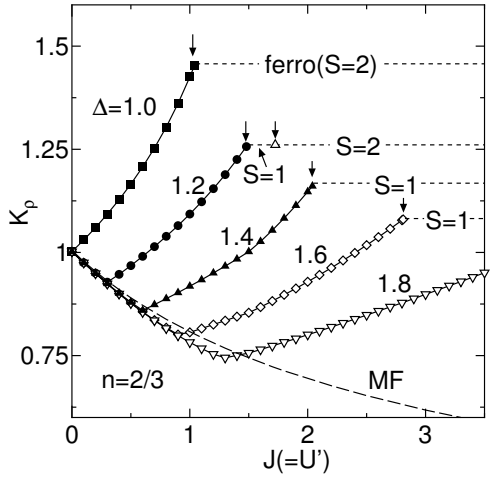

Figure 10: K_ρ as a function of $J(=U')$ for $n = 2/3$(6electrons/9sites) at $\Delta = 1.0, 1.2, 1.4, 1.6$, and 1.8. The down arrows indicate the critical points of $J(=U')$. The dashed line represents a weak coupling estimation for K_ρ.

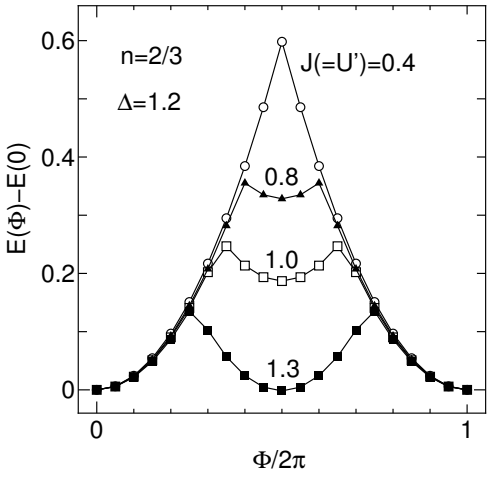

Figure 11: The energy difference $E_0(\phi) - E_0(0)$ as a function of an external flux ϕ for $J(=U')$ =0.4,0.8,1.0 and 1.3 at $n = 2/3$(6electrons/9sites) and $\Delta = 1.2$.

Figure 10 shows the value of K_ρ as a function of $J(=U')$ for several values of Δ at the electron density $n = 2/3$(6electrons/9sites). As J increases, K_ρ decreases for a small J, while it increases for a large J, and then becomes larger than unity. Since we consider the single component system, the SC correlation is expected to be the most dominant compared with the CDW and SDW correlations in the region $K_\rho > 1$. To confirm the superconducting state, we calculate the lowest energy of the singlet state $E_0(\phi)$ as a function of an external flux ϕ. As shown in Fig. 11, the anomalous flux quantization occurs clearly at $J \sim 1.3$, where K_ρ is about 1.1. When $J = 0.4$, K_ρ is less than unity and the anomalous flux quantization is not found.

When J is larger than a certain critical value, the ground state changes into the partially ferromagnetic state with S=1 or S=2 from the singlet state. In Fig. 10, the broken line represents the MF approximation for K_ρ. This approximation depends upon only the noninteracting ground state where the lower band is exclusively occupied, as shown in Fig. 1. Therefore, the effect of the upper

band is omitted and the result is independent of Δ. This approximation breaks down when the effect of the upper band becomes crucial. In this regime, K_ρ rapidly increases with increasing J, and finally becomes larger than unity indicating the superconducting state. The critical values of J with $K_\rho = 1$ are $J_c \approx 0.3$, 1.0, 2.4 and 4.0 for $\Delta = 1.0$, 1.2, 1.6 and 1.8, respectively.

In Fig.12, we show the phase diagram of the superconducting state with $K_\rho > 1$ together with the partial ferromagnetic state with $S = 1$ and $S = 2$ on the U' vs. J parameter plane for $n = 2/3$(6electrons/9sites) at $\Delta = 1.2$, where the $S = 2$ state is depicted by the bunch of thin solid circles(shadowed region). The superconducting phase appears near the partially polarized ferromagnetic region. It extends from the attractive region with $J < 0$ and $U' < 0$ to the realistic parameter region for $3d$ transition-metals with $U' > J > 0$. We have confirmed that the superconducting region increases as Δ decreases, as shown in Fig.10.

Figure 13 shows the global phase diagram on the $U' - J$ plane for $n = 4/3$(8electrons/6sites) at $\Delta = 4.0$. When $U' \gtrsim J \gtrsim \Delta$, the fully polarized ferromagnetism with $S = S_{\max}$ appears. It accompanies the partially polarized ferromagnetism with $0 < S < S_{\max}$ for $J \lesssim \Delta$. Inset shows the magnification of the phase diagram near the origin. As well as $n < 1$, the superconducting state with $K_\rho > 1$ appears near the partially polarized ferromagnetic region and it extends to the realistic parameter region with $U' > J > 0$. The configuration of the partially polarized ferromagnetic state and the superconducting state is similar to the case $n < 1$. When J exceeds $\epsilon^+(0) - E_{k_F}$, the interband excitation develops and the occupation number of the upper band increases, which results in a large orbital fluctuation accompanied by the fluctuation between the low-spin and the high-spin states. The mechanism of superconductivity may be related to this orbital fluctuation. We note that superconductivity is also observed for the $J' = 0$ ($J \neq 0$) case in contrast to the previous study[45, 46], where the pair-transfer J' is crucial to superconductivity. The existence of the partially polarized ferromagnetism for $\Delta > 0$ has been reported in a different type of two-band Hubbard model[40].

In Fig. 14, we show the doping dependence of the critical values of J for the superconductivity and the ferromagnetism at $\Delta = 4$ with $J = U'$, where we use n=4/3, 10/7, 3/2, 8/5 and 12/7 systems. We determine the critical values on condition that $K_\rho > 1$ for the superconductivity and $S > 0$ for the ferromagnetism. Although the finite size effect is considerably large, the phase boundary for the superconductivity can be approximately given by the phenomenological equation, $J_c = \epsilon^+(0) - E_{k_F}$. Here, $\epsilon^+(0) - E_{k_F}$ corresponds to the lowest energy of the single-particle excitation from the lower band to the upper band. This equation was found to be a good approximation for various $n > 1$[41].

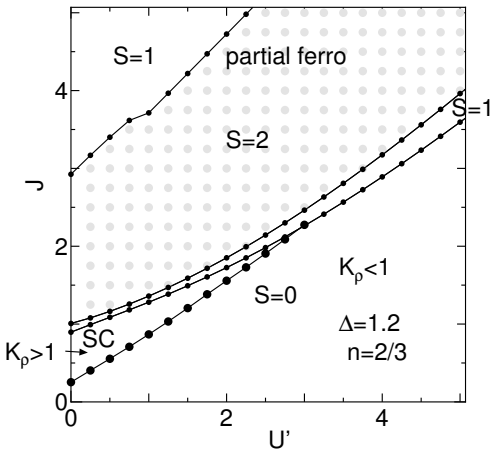

Figure 12: Phase diagram of the superconducting state with $K_\rho > 1$ and the ferromagnetic states with $S = 1$ and $S = 2$(shadowed region depicted by the bunch of thin solid circles) on the $U' - J$ parameter plane for $n = 2/3$(6electrons/9sites) at $\Delta = 1.2$.

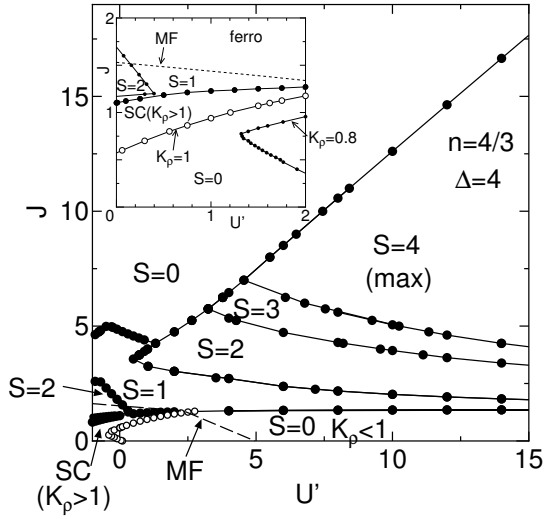

Figure 13: Global phase diagram on the $U' - J$ plane for $n = 8/6$ at $\Delta = 4.0$. The dashed line indicates the phase boundary of the complete(partial) ferromagnetic state obtained by the MF approximation. Inset shows the magnification of the phase diagram near the origin.

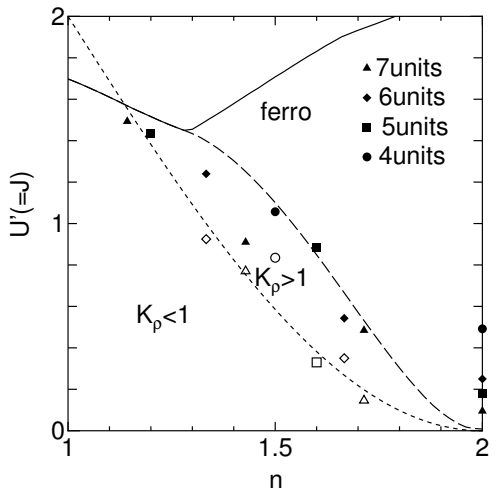

Figure 14: Phase diagram on the $n-J$ plane $\Delta = 4.0$. The broken line represents the phenomenological equation $J_c = \epsilon^+(0) - E_{k_F}$ (see text) as a function of n. The solid(dashed) line indicates the phase boundary of the complete(partial) ferromagnetic state obtained by the MF approximation.

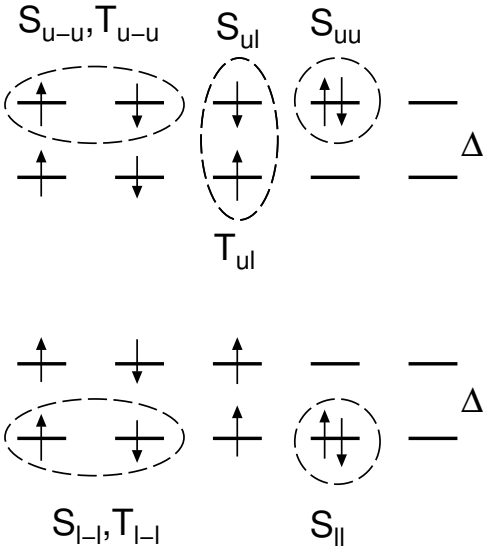

Figure 15: Schematic diagrams of various types of superconducting paring; $S_{\rm ll}$, $S_{\rm uu}$, $S_{\rm l-l}$, $S_{\rm u-u}$ and $S_{\rm ul}$(singlet paring) and $T_{\rm l-l(r)}$, $T_{\rm u-u}(r)$ and $T_{\rm ul}(r)$ (triplet paring)

We also show the phase boundary of the ferromagnetic state obtained by the MF approximation. It seems to consist with the numerical result.

3.4 Paring correlation functions

Next, we consider superconducting paring of the system, as shown in Fig. 15. In Fig.16, we show various types of superconducting paring correlation functions $C(r)$ in detail for $n = 2/3$(6electrons/9sites) at $\Delta = 1.0$ and $J(= U') = 1.04$. The paring correlation functions are defined by

$$S_{\rm ll}(r) = \frac{1}{N_u}\sum_i < c^\dagger_{i,l,\uparrow}c^\dagger_{i,l,\downarrow}c_{i+r,l,\downarrow}c_{i+r,l,\uparrow} >, \quad (6)$$

$$S_{\rm uu}(r) = \frac{1}{N_u}\sum_i < c^\dagger_{i,l,\uparrow}c^\dagger_{i,u,\downarrow}c_{i+r,u,\downarrow}c_{i+r,u,\uparrow} >, \quad (7)$$

$$S_{\rm l-l}(r) = \frac{1}{2N_u}\sum_i < (c^\dagger_{i,l,\uparrow}c^\dagger_{i+1,l,\downarrow} - c^\dagger_{i,l,\downarrow}c^\dagger_{i+1,l,\uparrow})(c_{i+r+1\downarrow}c_{i+r,l,\uparrow} - c_{i+r+1,l,\uparrow}c_{i+r,l,\downarrow}) >, \quad (8)$$

$$S_{\rm u-u}(r) = \frac{1}{2N_u}\sum_i < (c^\dagger_{i,u,\uparrow}c^\dagger_{i+1,u,\downarrow} - c^\dagger_{i,u,\downarrow}c^\dagger_{i+1,u,\uparrow})(c_{i+r+1,u,\downarrow}c_{i+r,u,\uparrow} - c_{i+r+1,u,\uparrow}c_{i+r,u,\downarrow}) >, \quad (9)$$

$$S_{\rm ul}(r) = \frac{1}{2N_u}\sum_i < (c^\dagger_{i,l,\uparrow}c^\dagger_{i+1,u,\downarrow} - c^\dagger_{i,l,\downarrow}c^\dagger_{i+1,u,\uparrow})(c_{i+r+1,u,\downarrow}c_{i+r,l,\uparrow} - c_{i+r+1,u,\uparrow}c_{i+r,l,\downarrow}) >, \quad (10)$$

$$T_{\rm l-l}(r) = \frac{1}{2N_u}\sum_i < (c^\dagger_{i,l,\uparrow}c^\dagger_{i+1,l,\downarrow} + c^\dagger_{i,l,\downarrow}c^\dagger_{i+1,l,\uparrow})(c_{i+r+1\downarrow}c_{i+r,l,\uparrow} + c_{i+r+1,l,\uparrow}c_{i+r,l,\downarrow}) >, \quad (11)$$

$$T_{\rm u-u}(r) = \frac{1}{2N_u}\sum_i < (c^\dagger_{i,u,\uparrow}c^\dagger_{i+1,u,\downarrow} + c^\dagger_{i,u,\downarrow}c^\dagger_{i+1,u,\uparrow})(c_{i+r+1,u,\downarrow}c_{i+r,u,\uparrow} + c_{i+r+1,u,\uparrow}c_{i+r,u,\downarrow}) >, \quad (12)$$

$$T_{\rm ul}(r) = \frac{1}{2N_u}\sum_i < (c^\dagger_{i,l,\uparrow}c^\dagger_{i+1,u,\downarrow} + c^\dagger_{i,l,\downarrow}c^\dagger_{i+1,u,\uparrow})(c_{i+r+1,u,\downarrow}c_{i+r,l,\uparrow} + c_{i+r+1,u,\uparrow}c_{i+r,l,\downarrow}) >, \quad (13)$$

where $C(r) = S_{\rm ll}(r)$, $S_{\rm uu}(r)$, $S_{\rm l-l}(r)$, $S_{\rm u-u}(r)$ and $S_{\rm ul}(r)$ denote the singlet paring correlation functions on the same site in the lower orbital, on the same site in the upper orbital, between the nearest neighbor sites in the lower orbital, between the nearest neighbor sites in the upper orbital, between lower and upper orbitals on the same site, respectively. Further, $T_{\rm l-l(r)}$, $T_{\rm u-u}(r)$ and $T_{\rm ul}(r)$ are the triplet paring correlation functions between the nearest neighbor sites in the lower orbital, between the nearest neighbor sites in the upper orbital and between lower and upper orbitals on the same site, respectively. The absolute value of $T_{\rm u-u}(r)$ is small, but the correlation of it is the slowest to decay. This result

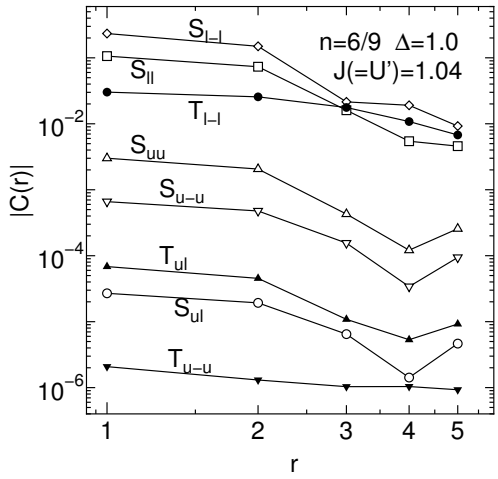

Figure 16: The singlet paring correlation functions $C(r) = S_{\rm ll}(r)$, $S_{\rm l-l}(r)$, $S_{\rm uu}(r)$, $S_{\rm u-u}(r)$, $S_{\rm ul}(r)$ and the triplet correlation functions $T_{\rm l-l}(r)$, $T_{\rm u-u}(r)$, $T_{\rm ul}(r)$, respectively(see text). Here we show the absolute value of the correlation functions at $\Delta = 1$ and $J(= U') = 1.04$ for n=2/3(6electrons/9sites).

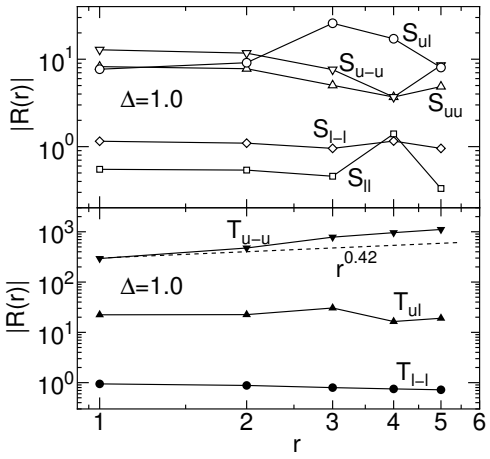

Figure 17: The ratio of the singlet paring correlation functions $R(r) = C(r)_{J=1.04}/C(r)_{J=0.2}$ for $S_{\rm l-l}(r)$, $S_{\rm uu}(r)$, $S_{\rm u-u}(r)$, $S_{ul}(r)$ and that of the triplet correlation functions for $T_{\rm l-l}(r)$, $T_{\rm u-u}(r)$, $T_{\rm ul}(r)$ with the power-low $r^{0.42}$, respectively(see text). The broken line represents the power-low $r^{0.42}$ predicted by the Luttinger liquid relation.

seems to suggest that the relevant paring of the superconductivity is the *tripletparing* between *lower* and *upper* orbitals on the same site and the ferromagnetic fluctuation near the ferromagnetic phase may cause the paring. To clarify the behavior of the correlation functions, we calculate the ratio $R(r)$ of the paring correlation functions at $J(= U') = 1.04$ and that of $J(= U') = 0.2$ as

$$R(r) = \frac{C(r)_{\rm J=1.04}}{C(r)_{\rm J=0.2}}. \tag{14}$$

Although the correlation function $C(r)$ decays as distance r increases, the function $R(r)$ for relevant paring is expected to increase with r, because the value of K_ρ at $J = 1.04$ is larger than that at $J = 0.2$, where K_ρ is about at 1.4 and 0.98, respectively. Then, the behavior of $R(r)$ is expected to $\sim r^{0.42}$. In fig.17, we show $R(r)$ for $S_{\rm ll}(r)$, $S_{\rm l-l}(r)$, $S_{\rm uu}(r)$, $S_{\rm u-u}(r)$ and $S_{\rm ul}$, (upper panel) and the triplet paring correlation functions $T_{\rm l-l}(r)$, $T_{\rm u-u}(r)$ and $T_{\rm ul}(r)$ with the power-low $r^{0.42}$ predicted by the Luttinger liquid relation (lower panel), respectively. It indicates that that function $R(r)$ for the triplet paring, $T_{\rm u-u}$, is much enhanced for long range paring correlation. On the other hand, the remains are not enhanced or decay as r increases. These results suggest that the paring correlation function $T_{\rm u-u}(r)$ is most relevant paring to the superconductivity. Although the system size is too small to compare the slope of the function $R(r)$ with the power-low enhancement $\sim r^{0.42}$ directly, the behavior of $R(r)$ for $T_{\rm u-u}(r)$ seems to be roughly consistent with the result of the Luttinger liquid relation.

4 *d-p* Chain Model

In the previous works[47, 48, 49, 50, 51, 52], the present authors and many other authors studied the one-dimensional *d-p* model with large on-site Coulomb repulsion U_d at Cu sites and intersite re-

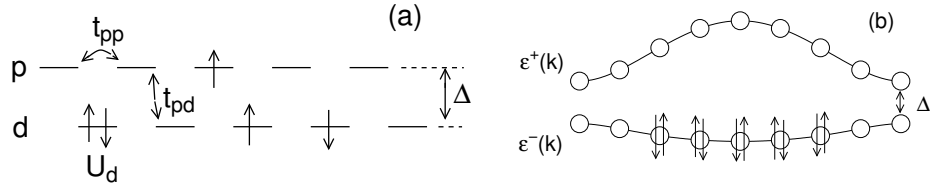

Figure 18: Schematic diagrams of (a) the model Hamiltonian and (b) the band structure in the noninteracting case.

pulsion U_{pd}, by using the numerical method. They claimed that the superconducting (SC) correlation is found to be dominant compared with the charge density wave (CDW) and spin density wave (SDW) correlations and the parameter U_{pd} is central in inducing a SC state. However, we found that if the hopping term t_{pp} is added to the model, the situation will be completely changed[53]. It enhances the fluctuation of charge and spin, and increases the exponent K_ρ as parameter U_{pd} does. Therefore, the repulsive interaction U_{pd} is not always necessary for the SC state.

In this section, we reexamine the one-dimensional d-p model in the presence of the hopping term t_{pp} to clarify the electronic structure of the SC state, especially paying attention to the symmetry of the paring correlation.

4.1 Model Hamiltonian

We consider the following model Hamiltonian for the Cu-O chain in the hole picture;

$$\begin{aligned} H &= t_{pd}\sum_{<ij>,\sigma}(p^\dagger_{i\sigma}d_{j\sigma}+h.c.)+t_{pp}\sum_{<ij>,\sigma}(p^\dagger_{i\sigma}p_{j\sigma}+h.c.) \\ &+ \epsilon_d\sum_{j,\sigma}d^\dagger_{j\sigma}d_{j\sigma}+\epsilon_p\sum_{i,\sigma}p^\dagger_{i\sigma}p_{i\sigma}+U_d\sum_j\hat{n}_{dj\uparrow}\hat{n}_{dj\downarrow}, \end{aligned} \tag{15}$$

where $d^\dagger_{j\sigma}$ and $p^\dagger_{i\sigma}$ stand for creation operators of a hole with spin σ in the Cu(d) orbital at site j and of a hole with spin σ in the O(p) orbital at site i, respectively, and $\hat{n}_{dj\sigma}=d^\dagger_{j\sigma}d_{j\sigma}$. Here, t_{pd} stands for the transfer energy between the nearest-neighbor d and p sites and will be set at unity (t_{pd}=1) hereafter in this study. The atomic energy levels of d orbital and p orbital are given by ϵ_d and ϵ_p, respectively. The charge-transfer energy Δ is defined as $\Delta=\epsilon_p-\epsilon_d$.

For the noninteracting case ($U_d=0$), the Hamiltonian in eq. (15) is easily diagonalized to yield a dispersion relation

$$E^\pm(k)=\frac{1}{2}\Big\{\epsilon_d+\epsilon_p+2t_{pp}\cos k\pm\sqrt{(\Delta+2t_{pp}\cos k)^2+16(t_{pd}\cos(k/2))^2}\Big\}, \tag{16}$$

where k is a wave vector and $E^+(k)(E^-(k))$ represent an upper (lower) band energy. For $t_{pp}>0$, the width of the lower band $E^-(k)$ decreases with decreasing Δ and becomes perfectly flat at $\Delta_{flat}=2t_{pp}-t^2_{pd}/t_{pp}$. When $\Delta<\Delta_{flat}$, the band bends with a peak at $k=0$. To investigate the electronic structure of the interacting case, we numerically diagonalize the Hamiltonian up to 14 sites (7 unit cells). To carry out a systematic calculation, We use the periodic boundary condition for $N_h=4m+2$ and the antiperiodic boundary condition for $N_h=4m$, where N_h is the total hole number and m is an integer.

4.2 Critical exponent K_ρ

In Fig. 19, we show the numerical results of K_ρ obtained through eq. 2 as a function of U_d for $n=4/3$(8holes/6units) at $\Delta=2$ and $t_{pp}=0.5$. We also plot K_ρ obtained through the mean field (MF) approximation, respectively. In the MF approximation, the renormalized bands $\tilde{E}^\pm(k)$ are given by eq. 16 in which Δ is replaced by

$$\tilde{\Delta}=\Delta-\frac{1}{2}U_d<n_d>, \tag{17}$$

where $<n_d>$ is the hole density at a d site and is determined by solving the self-consistent equation in the MF approximation. Using the renormalized band $\tilde{E}^-(k)$, we can calculate the charge susceptibility

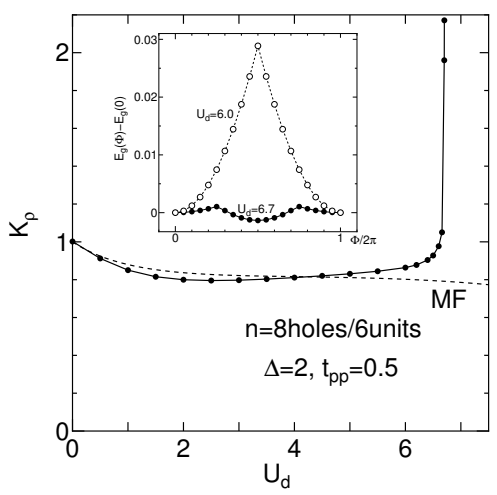

Figure 19: The critical exponent K_ρ as a function of U_d at $\Delta = 2$ and $t_{pp} = 0.5$ for $n = 4/3$(8holes/6units). The dashed lines represent the results of the MF approximation (See in the text) Inset shows the energy difference $E_0(\phi) - E_0(0)$ as a function of an external flux ϕ

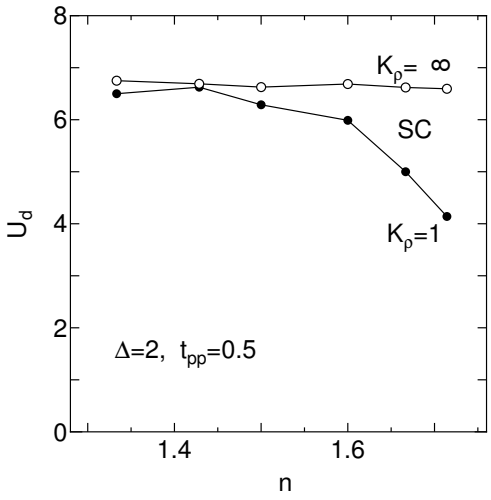

Figure 20: The SC region sandwiched between the two lines of $K_\rho = 1$ and $K_\rho = \infty$ on the n-U_d parameter plane at $\Delta = 2$ and $t_{pp} = 0.5$. Here, we use $n = 8/6, 10/7, 6/4, 8/5$, 10/6 and 12/7 systems.

χ_c and the Drude weight D. Substituting those values into eq. (2), we obtain K_ρ within the MF approximation. In the weak coupling regime, the results of the numerical diagonalization are in good agreement with the MF approximation. It also seems to be roughly consistent with the numerical results even in the strong coupling regime except for $U_d \gtrsim 6$.

When $U_d \lesssim 3$, K_ρ decreases as U_d increases. For sufficiently large U_d, K_ρ increases with increasing U_d and diverges at $U_d \sim 6.8$ when the charge susceptibility diverges. The region where K_ρ is larger than unity appears at $6.5 \lesssim U_d \lesssim 6.8$. When $K_\rho > 1$, the SC correlation is expected to be most dominant compared with the CDW and SDW correlations. Inset shows the energy difference $E_0(\phi) - E_0(0)$ as a function of an external flux ϕ. It shows that the anomalous flux quantization occurs at $U_d = 6.7$, when K_ρ is about 2.0. While, at $U_d = 6.0$, $K_\rho \simeq 0.86$ and the anomalous flux quantization is not found. These result also confirms the SC phase at $U_d = 6.7$. The divergence of K_ρ suggests that the effective bandwidth is close to zero. In fact, if we use the numerical value of $< n_d > \simeq 0.83$ with $U_d = 6.7$ in eq. (7), we obtain $\tilde{\Delta} \sim -0.8$ and the effective bandwidth is nearly equal to 0.1. It is very small compared with the noninteracting band. The result of the anomalous flux quantization shows that the variation of $|E_0(\phi) - E_0(0)|$ at $U_d = 6.7$ is much smaller than that at $U_d = 6.0$. It also indicates that the effective bandwidth is small.

Figure 20 shows the SC region where $1 < K_\rho < \infty$ on the $n - U_d$ parameter plane at $\Delta = 2$ and $t_{pp} = 0.5$. We use $n = 8/6, 10/7, 6/4, 8/5$, 10/6 and 12/7 systems, where numerator and denominate correspond to numbers of electrons and unit cells, respectively. The region sandwiched between the two lines of $K_\rho = 1$ and $K_\rho = \infty$ corresponds to the SC region. It is narrow near $n = 1.4$, however, it increases with increasing n.

4.3 Paring correlation functions

We investigate various types of superconducting paring in detail. as shown in Fig. 21. Figure 22 shows the paring correlation functions $C(r)$ defined by

$$S_{\mathrm{p-on}}(r) = \frac{1}{N_u}\sum_i < p^\dagger_{i\uparrow} p^\dagger_{i\downarrow} p_{i+r\uparrow} p_{i+r\downarrow} >, \tag{18}$$

$$S_{\mathrm{d-on}}(r) = \frac{1}{N_u}\sum_i < d^\dagger_{i\uparrow} d^\dagger_{i\downarrow} d_{i+r\uparrow} d_{i+r\downarrow} >, \tag{19}$$

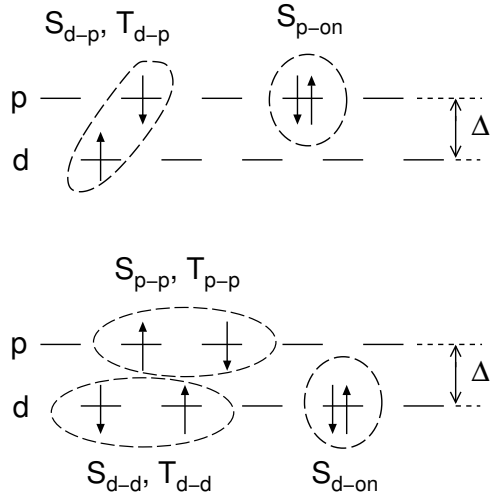

Figure 21: Schematic diagrams of various paring for d-p model.

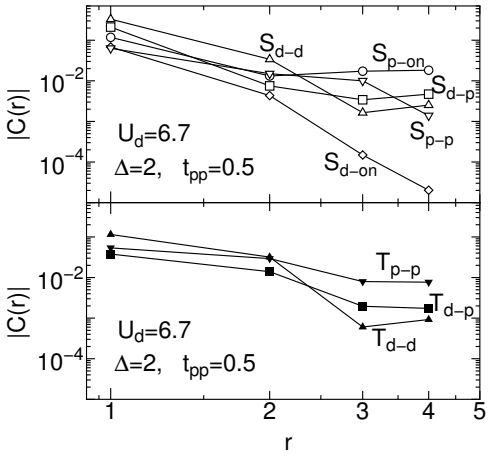

Figure 22: The singlet paring correlation functions $C(r) = S_{\rm p-on}(r)$, $S_{\rm p-p}(r)$, $S_{\rm d-on}(r)$, $S_{\rm d-d}(r)$ and $S_{\rm d-p}(r)$ (upper panel) and the triplet paring correlation functions $T_{\rm p-p}(r)$, $T_{\rm d-d}(r)$ and $T_{\rm d-p}(r)$ (lower panel), respectively (see text). Here we show the absolute value of the correlation functions at $\Delta = 2$, $t_{pp} = 0.5$ and $U_d = 6.7$ for n=4/3(8holes/6units).

$$S_{\rm p-p}(r) = \frac{1}{2N_u}\sum_i < (p^\dagger_{i\uparrow}p^\dagger_{i+1\downarrow} - p^\dagger_{i\downarrow}p^\dagger_{i+1\uparrow})(p_{i+r+1\downarrow}p_{i+r+1\uparrow} - p_{i+r+1\uparrow}p_{i+r\downarrow}) >, \quad (20)$$

$$S_{\rm d-d}(r) = \frac{1}{2N_u}\sum_i < (d^\dagger_{i\uparrow}d^\dagger_{i+1\downarrow} - d^\dagger_{i\downarrow}d^\dagger_{i+1\uparrow})(d_{i+r+1\downarrow}d_{i+r+1\uparrow} - d_{i+r+1\uparrow}d_{i+r\downarrow}) >, \quad (21)$$

$$S_{\rm d-p}(r) = \frac{1}{2N_u}\sum_i < (d^\dagger_{i\uparrow}p^\dagger_{i\downarrow} - d^\dagger_{i\downarrow}p^\dagger_{i\uparrow})(p_{i+r\downarrow}d_{i+r\uparrow} - p_{i+r\uparrow}d_{i+r\downarrow}) >, \quad (22)$$

$$T_{\rm p-p}(r) = \frac{1}{2N_u}\sum_i < (p^\dagger_{i\uparrow}p^\dagger_{i+1\downarrow} + p^\dagger_{i\downarrow}p^\dagger_{i+1\uparrow})(p_{i+r+1\downarrow}p_{i+r+1\uparrow} + p_{i+r+1\uparrow}p_{i+r\downarrow}) >, \quad (23)$$

$$T_{\rm d-d}(r) = \frac{1}{2N_u}\sum_i < (d^\dagger_{i\uparrow}d^\dagger_{i+1\downarrow} + d^\dagger_{i\downarrow}d^\dagger_{i+1\uparrow})(d_{i+r+1\downarrow}d_{i+r+1\uparrow} + d_{i+r+1\uparrow}d_{i+r\downarrow}) >, \quad (24)$$

$$T_{\rm d-p}(r) = \frac{1}{2N_u}\sum_i < (d^\dagger_{i\uparrow}p^\dagger_{i\downarrow} + d^\dagger_{i\downarrow}p^\dagger_{i\uparrow})(p_{i+r\downarrow}d_{i+r\uparrow} + p_{i+r\uparrow}d_{i+r\downarrow}) >, \quad (25)$$

where $S_{\rm p-on}(r)$, $S_{\rm d-on}(r)$, $S_{\rm p-p}(r)$, $S_{\rm d-d}(r)$ and $S_{\rm d-p}(r)$ denote the singlet paring correlation functions on a same p site, on a same d site, between the nearest neighbor p sites, between the nearest neighbor d sites and between the nearest neighbor p and d sites, respectively. Further, $T_{\rm p-p}(r)$, $T_{\rm d-d}(r)$ and $T_{\rm d-p}(r)$ denote the triplet paring correlation functions between the nearest neighbor p sites, between the nearest neighbor d sites and between the nearest neighbor p and d sites, respectively. Here, we show the absolute value of the correlation functions at $\Delta = 2$, $t_{pp} = 0.5$ and $U_d = 6.7$ for n=4/3(8holes/6units). The orders of the absolute value of these correlation functions are almost equal to one another.

However, the correlation functions C(r) for $S_{\rm p-on}(r)$ and $S_{\rm p-p}(r)$ seem to decay slower than that of the remains. It suggests that these paring play an important role in the superconductivity. We also examine the ratio of the paring correlation functions $R(r)$ at $U_d = 6.7$ and $U_d = 6.0$ as $R(r) = C(r)_{U_d=6.7}/ = C(r)_{U_d=6.0}$, where $K_\rho \sim 2.0$ at $U_d = 6.7$ and $K_\rho \sim 0.86$ at $U_d = 6.0$. The function $R(r)$ for relevant paring is expected to behave as $r^{1.1}$. In fig.23, we show the ratio of the paring correlation functions $R(r)$ for $S_{\rm p-on}(r)$, $S_{\rm p-p}(r)$, $S_{\rm d-on}(r)$, $S_{\rm d-d}(r)$ and $S_{\rm d-p}(r)$ with the power-low $r^{1.1}$ (upper panel) and that of the triplet paring correlation functions for $T_{\rm p-p}(r)$, $T_{\rm d-d}(r)$

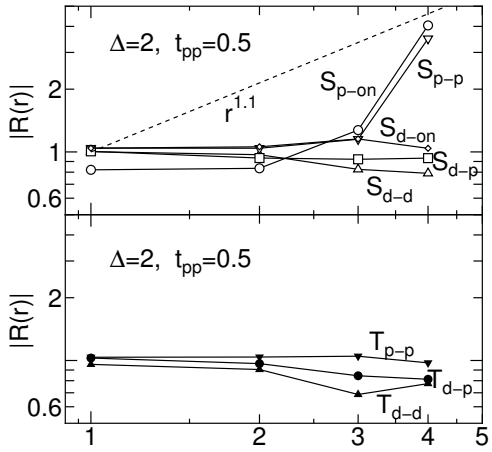

Figure 23: The ratio of the singlet paring correlation functions $R(r) = C(r)_{U_d=6.7}/C(r)_{U_d=6.0}$ for $S_{\mathrm{p-on}}(r)$, $S_{\mathrm{p-p}}(r)$, $S_{\mathrm{d-on}}(r)$, $S_{\mathrm{d-d}}(r)$ and $S_{\mathrm{d-p}}(r)$ with the power-low $r^{1.1}$ depicted the broken line (upper panel) and that of the triplet paring correlation functions for $T_{\mathrm{p-p}}(r)$, $T_{\mathrm{d-d}}(r)$ and $T_{\mathrm{d-p}}(r)$ (lower panel), respectively. Here we show the absolute value of $R(r)$ at $\Delta = 2$, $t_{pp} = 0.5$ for n=4/3(8holes/6units).

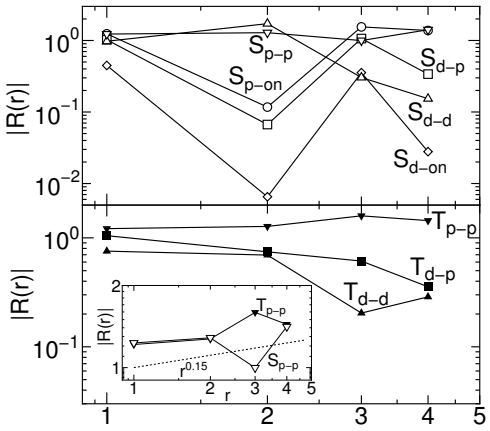

Figure 24: The ratio of the singlet paring correlation functions $R(r) = C(r)_{U_d=6.59}/C(r)_{U_d=4.14}$ for $S_{\mathrm{p-on}}(r)$, $S_{\mathrm{p-p}}(r)$, $S_{\mathrm{d-on}}(r)$, $S_{\mathrm{d-d}}(r)$ and $S_{\mathrm{d-p}}(r)$(upper panel), and that of the triplet paring correlation functions for $T_{\mathrm{p-p}}(r)$, $T_{\mathrm{d-d}}(r)$ and $T_{\mathrm{d-p}}(r)$ (lower panel), respectively. Here we show the absolute value of $R(r)$ at $\Delta = 2$, $t_{pp} = 0.5$ for n=12/7(12holes/7units). Inset shows $R(r)$ for $S_{\mathrm{p-p}}(r)$ and $T_{\mathrm{p-p}}(r)$ with the power-low $r^{0.15}$.

and $T_{\mathrm{d-p}}(r)$ (lower panel), respectively. It indicates that that $R(r)$ for $S_{\mathrm{p-on}}(r)$ and $S_{\mathrm{p-p}}(r)$ are much enhanced at long range paring correlation and seem to be roughly consistent with the power-low obtained by the Luttinger liquid relation. On the other hand, the remains decay as distance r increases or are almost constant. These results suggest that the singlet paring correlation functions $S_{\mathrm{p-on}}(r)$ and $S_{\mathrm{p-p}}(r)$ are most relevant to the superconductivity and the triplet paring is irrelevant.

On the other hand, the situation is changed for large hole density. In this case, the triplet paring correlation is enhanced as well as the singlet paring correlation. In fig.24, we show the ratio of the singlet paring correlation functions $R(r) = C(r)_{U_d=6.59}/C(r)_{U_d=4.14}$ for $S_{\mathrm{p-on}}(r)$, $S_{\mathrm{p-p}}(r)$, $S_{\mathrm{d-on}}(r)$, $S_{\mathrm{d-d}}(r)$ and $S_{\mathrm{d-p}}(r)$ (upper panel), and that of the triplet paring correlation functions for $T_{\mathrm{p-p}}(r)$, $T_{\mathrm{d-d}}(r)$ and $T_{\mathrm{d-p}}(r)$(lower panel), respectively, where we show the absolute value of $R(r)$ for n=12/7(12holes/7units). Here, $R(r)$ of the relevant paring is expected to behave as $r^{0.15}$ since $K_\rho \sim 1.15$ at $U_d = 6.59$ and $K_\rho \sim 1.0$ at $U_d = 4.14$. Inset shows $R(r)$ for $S_{\mathrm{p-p}}(r)$ and $T_{\mathrm{p-p}}(r)$ with the power-low $r^{0.15}$. It shows that $R(r)$ for $T_{\mathrm{p-p}}(r)$ increases with r as well as that for $S_{\mathrm{p-p}}(r)$, which seems to be roughly consistent with the power-low $r^{0.15}$ predicted by the Luttinger liquid relation. suggests that the triplet paring becomes relevant to the superconductivity as well as the singlet paring near $n = 2$.

5 d-p Model in Infinite Dimensions

Recently, some significant progress has been achieved in understanding the strongly correlated electron systems by using the dynamical mean-field theory (DMFT)[54, 55]. In this approach, the lattice problem is mapped onto an effective impurity problem where a correlated impurity site is embedded in an effective uncorrelated medium that has to be determined self-consistently. To solve the effective impurity problem, several methods have been applied including the iterated perturbation theory[55], the non-crossing approximation[56], the quantum Monte Carlo (QMC) method[57], the exact diagonalization (ED) method[58] and the numerical renormalization group (NRG) method[59, 60]. The DMFT becomes exact in the limit of infinite spatial dimensions ($d = \infty$)[54] and believed to be a good approximation in high dimensions.

In the $d = \infty$ single-band Hubbard model at half-filling, the Mott metal-insulator transition is found to occur as a first-order phase transition at finite temperature below a critical temperature $T_{\rm cr}$[55]. Below $T_{\rm cr}$, a coexistence of the metallic and insulating solutions is found for the same value of the on-site Coulomb interaction U in the range $U_{c1} < U < U_{c2}$[55, 60]. The magnetic phase diagram was obtained as a function of doping, temperature and U. A commensurate antiferromagnetic order changes to an incommensurate state at a value of the doping which depends on U[61]. The ferromagnetism was observed for an intermediate interaction strength $U \gtrsim 2$ in non-bipartite lattices such as the fcc-type lattice[62] but was completely suppressed for $U \lesssim 20$ in bipartite lattices such as the hypercubic lattice[63]. The superconducting phase is absent in the $d = \infty$ single-band Hubbard model[64].

The DMFT has also been applied to the multi-band Hubbard model to elucidate the effect of the Hund's rule coupling on the Ferromagnetism[20, 22] and the Mott transition[65, 66]. Several authors have extensively studied the *d-p* model using the DMFT[58, 67, 68, 69, 70, 71, 72, 73, 74, 75]. The Mott transition was found to occur at $n = 1$ (or $n = 3$)[67, 68, 69, 70, 71, 73, 74], where n is the total electron number per unit cell and given by the sum of p- and d-electron numbers: $n = n_p + n_d$. The phase diagram of the Mott transition was obtained over the whole parameter regime including the Mott-Hubbard type ($U < \Delta$) and the charge-transfer type ($U > \Delta$)[69, 70]. When the carrier is doped with $n > 1$, the superconductivity was observed in the charge-transfer regime[58, 67, 69], while it was not observed in the Mott-Hubbard regime. The antiferromagnetism was also observed at and near $n = 1$[75]. More recently, the present authors discussed the ferromagnetism which was found to occur at and near $n = 2$ in the intermediate interaction strength $U \approx 2\Delta \gtrsim 2$[72]. Therefore it is interesting to discuss the relationship between the magnetism and the superconductivity in the *d-p* model in infinite dimensions and to obtain the phase diagram as functions of the parameters such as the interaction, the electron filling and the temperature.

5.1 Model and formulation

We consider the *d-p* model on a Bethe lattice with infinite connectivity $z \to \infty$. The Hamiltonian is written as

$$H = \sum_{i,j,\sigma} (t_{i,j} d^\dagger_{i\sigma} p_{j\sigma} + h.c.) + \epsilon_p \sum_{j,\sigma} p^\dagger_{j\sigma} p_{j\sigma} + \epsilon_d \sum_{i,\sigma} d^\dagger_{i\sigma} d_{i\sigma} + U_d \sum_i n^d_{i\uparrow} n^d_{i\downarrow}, \tag{26}$$

where $d^\dagger_{i\sigma}$ and $p^\dagger_{j\sigma}$ stand for creation operators of a electron (or a hole) with spin σ in the d-orbital at site i and in the p-orbital at site j, respectively. $n^d_{i,\sigma} = d^\dagger_{i\sigma} d_{i\sigma}$. $t_{i,j} = \frac{t_{pd}}{\sqrt{z}}$ represents the transfer energy between the nearest neighbor site and the parameter t_{pd} will be set to unity in the present study. The atomic energy levels of d-orbital and p-orbital are given by ϵ_d and ϵ_p, respectively. The charge-transfer energy Δ is defined as $\Delta = \epsilon_p - \epsilon_d > 0$.

In the DMFT, the effective action of the impurity problem is given by

$$S = U_d \int_0^\beta d\tau n_{d\uparrow}(\tau) n_{d\downarrow}(\tau) - \int_0^\beta \int_0^\beta d\tau d\tau' \sum_\sigma d^\dagger_\sigma(\tau) D^{-1}_{0\sigma}(\tau - \tau') d_\sigma(\tau'), \tag{27}$$

where the Weiss function $D_{0\sigma}$ includes effects of the interaction at all the sites except the impurity site. This action is derived by tracing out the fermionic degrees of freedom in the original lattice model except the impurity site. The local Green's function $D_\sigma(\tau - \tau') = -\langle T d_\sigma(\tau) d^\dagger_\sigma(\tau') \rangle_S$ is calculated with this action. Using $D_{0\sigma}$ and D_σ, we introduce the local self-energy $\Sigma_\sigma(i\omega_n) = D_{0\sigma}(i\omega_n)^{-1} - D_\sigma(i\omega_n)^{-1}$, where ω_n is the Matsubara frequency, $\omega_n = (2n+1)\pi/\beta$. The self-consistency condition for the local Green's functions gives the relations

$$D_\sigma(i\omega_n) = \int d\varepsilon N(\varepsilon) \times \frac{i\omega_n + \mu - \varepsilon_p}{(i\omega_n + \mu - \varepsilon_d - \Sigma_\sigma(i\omega_n))(i\omega_n + \mu - \varepsilon_p) - \varepsilon^2}, \tag{28}$$

$$P_\sigma(i\omega_n) = \int d\varepsilon N(\varepsilon) \times \frac{i\omega_n + \mu - \varepsilon_d - \Sigma_\sigma(i\omega_n)}{(i\omega_n + \mu - \varepsilon_d - \Sigma_\sigma(i\omega_n))(i\omega_n + \mu - \varepsilon_p) - \varepsilon^2}, \tag{29}$$

where μ is the chemical potential and $P_\sigma(\tau - \tau') = -\langle T p_\sigma(\tau) p^\dagger_\sigma(\tau') \rangle_S$ is the local Green's function at p-site. For the Bethe lattice with $z = \infty$, the density of states is given by a semi-circular function,

$N(\varepsilon) = \sqrt{4-(\varepsilon/t_{pd})^2}/2\pi t_{pd}$. Using the semi-circular density of states in eqs.(28) and (29) and eliminating $\Sigma_\sigma(i\omega_n)$, we obtain the simple form of the self-consistency equations

$$D_{0\sigma}(i\omega)^{-1} = i\omega_n + \mu - \varepsilon_d - t_{pd}^2 P_\sigma(i\omega_n), \tag{30}$$

$$P_\sigma(i\omega)^{-1} = i\omega_n + \mu - \varepsilon_p - t_{pd}^2 D_\sigma(i\omega_n). \tag{31}$$

To calculate the local Green's function $D_\sigma(i\omega_n)$ for a given $D_{0\sigma}(i\omega_n)$, we use the numerical diagonalization method (DMFT-ED method). The self-consistency equations (30) and (31) lead a new $D_{0\sigma}(i\omega)$ and we repeat the calculation of the local Green's function. This process is iterated until the solutions converge.

In the DMFT-ED method, we approximately solve the impurity Anderson model of a finite-size cluster;

$$H_{And} = \varepsilon_{0\sigma}\sum_\sigma n_{d\sigma} + \sum_{l=2,\sigma}^{N_s} \varepsilon_{l\sigma} c_{l\sigma}^\dagger c_{l\sigma} + \sum_{l=2,\sigma}^{N_s} V_{l\sigma}(d_\sigma^\dagger c_{l\sigma} + c_{l\sigma}^\dagger d_\sigma) + U_d n_{d\uparrow} n_{d\downarrow}, \tag{32}$$

where $\varepsilon_{0\sigma}$ is the impurity level and $\varepsilon_{l\sigma}$ $(l = 2, 3, ..., N_s)$ are levels of the 'conduction electron' hybridized with the impurity by $V_{l\sigma}$. We regard the non-interacting Green's function $G_{0\sigma}^{And}(i\omega_n)$ as the Weiss function $D_{0\sigma}(i\omega)$ in the action eq.(27). Then, the interacting Green's function $G_\sigma^{And}(i\omega_n)$ corresponds to the local Green's function $D_\sigma(i\omega)$ in the original lattice problem. Here, $G_{0\sigma}^{And}(i\omega_n)$ is defined by

$$G_{0\sigma}^{And}(i\omega_n) = \frac{1}{i\omega_n - \varepsilon_{0\sigma} - \sum_{l=2}^{N_s} \frac{V_{l\sigma}^2}{i\omega_n - \varepsilon_{l\sigma}}}. \tag{33}$$

For a given $D_{0\sigma}(i\omega)$, we determine $2N_s - 1$ parameters $\varepsilon_{0\sigma}, \varepsilon_{l\sigma}, V_{l\sigma} (l = 2, 3, ..., N_s)$ to make $G_{0\sigma}^{And}(i\omega_n)$ as close to $D_{0\sigma}(i\omega)$ as possible. Using these parameters, we diagonalize the finite cluster of the impurity Anderson model, and calculate $G_{0\sigma}^{And}(i\omega_n)$ $(D_{0\sigma}(i\omega_n))$. At finite temperature, the Green's function is straightforwardly calculated from the full set of states $|i\rangle$ with eigenvalues E_i according to

$$D_\sigma(i\omega_n) = \frac{1}{Z}\sum_{i,j} \frac{|\langle i|d_\sigma^\dagger|j\rangle|^2}{i\omega_n - E_i + E_j}(\mathrm{e}^{-\beta E_i} + \mathrm{e}^{-\beta E_j}). \tag{34}$$

Using the Lanczos method with the continued-fraction expansions, we also calculate the zero temperature Green's functions. In this case, we replace the Matsubara frequencies by a fine grid of imaginary frequencies, $\tilde{\beta}$ $(i\omega_n = (2n+1)\pi/\tilde{\beta})$, where the fictitious inverse temperature $\tilde{\beta}$ determines a low-frequency cut-off.

5.2 Metal-Insulator transition at $n = 2$

First, we consider the paramagnetic state at zero temperature for $n = n_d + n_p = 2$. In the non-interacting case $U_d = 0$, the system is a band-insulator with the energy gap Δ for $\Delta \neq 0$ while it is a semimetal for $\Delta = 0$. Within the restricted Hartree-Fock (HF) approximation, the energy gap is given by $\Delta - \frac{U_d n_d}{2}$. Then the system is metallic for $U_d = 2\Delta$, otherwise it is insulating. We note that $n_d = n_p = 1$ for $U_d = 2\Delta$ due to the particle-hole symmetry. In the inset in Fig. 25, we show the chemical potential μ as functions of n for $U_d = 7, 8, 9, 10$ at $\Delta = 6$ and $T = 0$ calculated from the DMFT-ED method with the system size $N_s = 8$[72]. In this calculation, the solution is restricted to the paramagnetic state with $\varepsilon_{0\sigma} = \varepsilon_0$, $\varepsilon_{l\sigma} = \varepsilon_l$ and $V_{l\sigma} = V_l$ for $l = 2, 3, ..., N_s$. When U_d increases from $U_d = 0$, the discontinuity in the chemical potential at $n = 2$ decreases and finally becomes zero at a critical value, where a transition from the band-insulator to the correlated semimetal occurs[67]. The critical values for the metal-insulator transition are plotted in Fig. 25. In contrast to the HF approximation, the metallic state is found in the wide parameter region due to a correlation effect considered in the DMFT.

5.3 Ferromagnetism

At low temperature, the correlated semimetal mentioned above becomes unstable compared to a ferromagnetic state. In Fig. 26, we plot the magnetization for the d-electron M_d, that for the p-electron M_p and the total magnetization $M = M_d + M_p$ as functions of the temperature T at $n = 2$ for $U_d = 8$

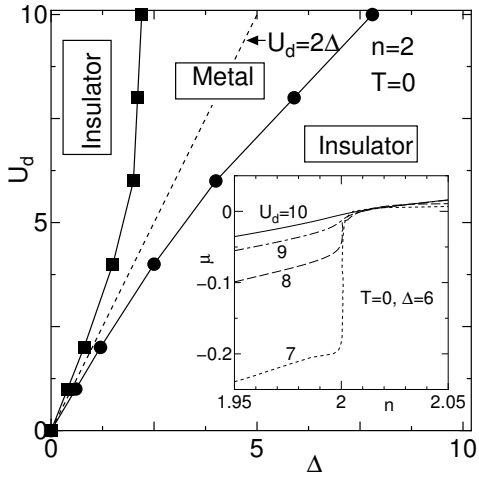

Figure 25: The phase boundary separating the metallic and insulating regimes as a function of U_d and Δ at $n = 2$ and $T = 0$. The inset shows the chemical potential as functions of n for $U_d = 7, 8, 9, 10$ at $\Delta = 6$ and $T = 0$ calculated from the DMFT-ED method with $N_s = 8$.

and $\Delta = 4$ calculated from the DMFT-ED method with $N_s = 6$[72]. As shown in Fig. 26, M_d and M_p have opposite sign to each other. In the low temperature limit, both of M_d and M_p become constant, while the sum of them M becomes zero. The feature of the ferromagnetism from the DMFT is similar to that from the HF approximation as shown in Fig. 26. However, the transition temperature T_c from the HF approximation is much higher than that from the DMFT (see also Fig. 29). In Fig. 27, we plot the magnetization as functions of U_d with keeping $\Delta = \frac{U_d}{2}$ at $n = 2$ and $T = 0.01$ calculated from the DMFT-ED method together with those from the HF approximation. When U_d increases, the each component of the magnetization monotonically increases. In both approximations, the ferromagnetism is observed for the intermediate interaction strength $U_d \gtrsim 2$. This is a striking contrast to the single-band Hubbard model where the ferromagnetism is observed only for the strong

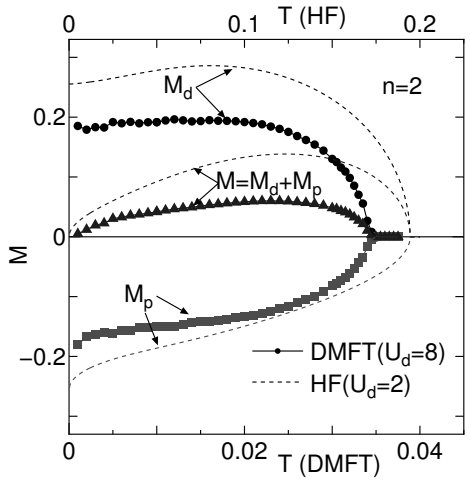

Figure 26: The magnetization for the d-electron M_d, that for the p-electron M_p and the total magnetization $M = M_d + M_p$ as functions of the temperature T at $n = 2$, obtained from the DMFT-ED method for $U_d = 8$ and $\Delta = 4$ with $N_s = 6$ and from the HF approximation (dashed lines) for $U_d = 2$ and $\Delta = 1$.

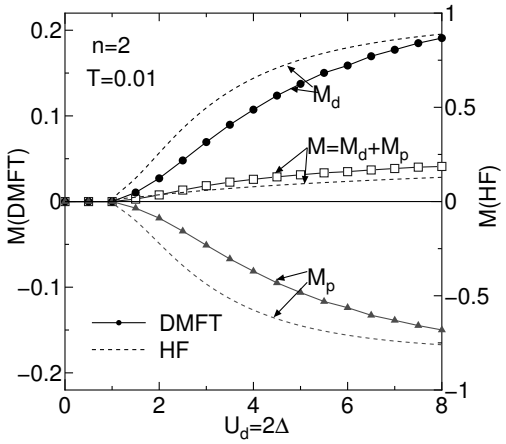

Figure 27: The magnetization for the d-electron M_d, that for the p-electron M_p and the total magnetization $M = M_d + M_p$ as functions of U_d with $\Delta = U_d/2$ at $n = 2$ and $T = 0.01$, obtained from the DMFT-ED method and from the HF approximation (dashed lines).

coupling region $U \gtrsim 20$ in bipartite lattices within the DMFT[63]. We note that the value of the magnetization from the DMFT is about five times smaller than that from the HF for the same values of U_d and Δ.

Fig. 28 shows the total magnetization M as a function of the electron filling n. When n decreases, M continuously becomes zero at a critical value of n for high temperatures (see for $T = 0.025$), while it discontinuously becomes zero for low temperatures (see for $T = 0.01$). The similar properties are also observed within the HF approximation as shown in Fig. 28. At low temperatures, however, the HF approximation also predicts a metastable state where M decreases with increasing n and continuously becomes zero at a critical n (see for $T = 0.025$). By calculating the thermodynamic potential, we find that the phase separation of the ferromagnetic state and the paramagnetic state occurs at the low temperatures (see Fig. 29).

Fig. 29 shows the transition temperature for the ferromagnetism T_c as a function of n for several values of $U_d(= 2\Delta)$[72]. T_c monotonically decreases with decreasing n. The closed circles show the second-order phase transition, while the open circles show the discontinuous transition as seen in Fig. 28. Within the HF approximation, the second-order phase transition occurs at the high temperature (solid line), while the phase separation occurs at the low temperature (area between the dotted lines). In the DMFT, it is difficult to calculate the thermodynamic potential directly from the local Green's function. But we may expect that, within the DMFT, the similar phase separation takes place at low temperatures where the magnetization shows a discontinuous transition as shown in Fig. 28.

5.4 Superconductivity

Finally, we discuss the superconductivity in the *d-p* model (26). In infinite dimensions, the on-site paring susceptibility χ of this model is given by[55, 67]

$$\begin{aligned} \chi &= \frac{1}{N}\int_0^\beta d\tau \sum_{ij} < T d_{i\uparrow}(\tau) d_{i\downarrow}(\tau) d^\dagger_{j\downarrow}(0) d^\dagger_{j\uparrow}(0) > \\ &= T\sum_{\nu,\nu'} [\alpha^{-1/2}\{I-\Lambda\}^{-1}\cdot\Lambda\cdot\alpha^{-1/2}]_{\nu,\nu'}, \end{aligned} \tag{35}$$

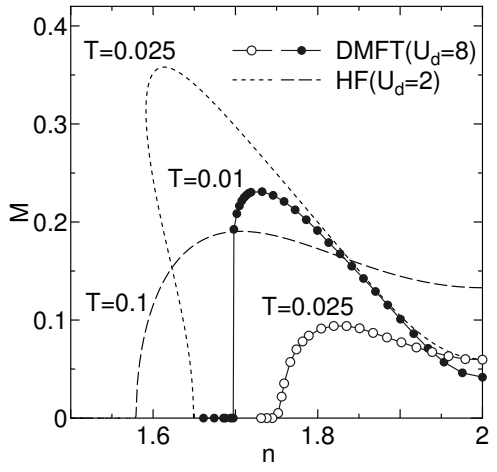

Figure 28: The total magnetization M as a function of the electron number n, obtained from the DMFT-ED method for $U_d = 8$ and $\Delta = 4$ at $T = 0.01$ (closed circles), 0.025 (open circles), and from the HF approximation for $U_d = 2$ and $\Delta = 1$ at $T = 0.025$ (dotted line), 0.1 (dashed line).

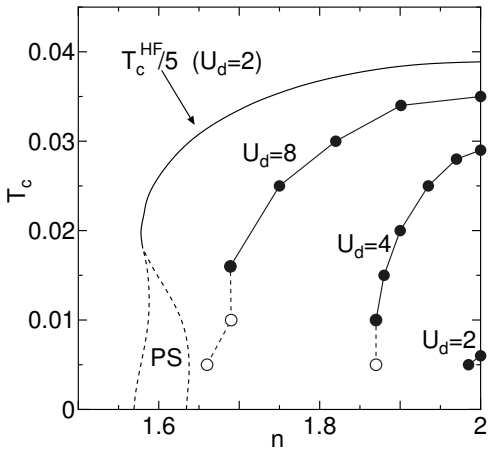

Figure 29: The transition temperature T_c for the ferromagnetism as a function of the electron filling n, obtained from the DMFT-ED method (closed and open circles) for $U_d = 2\Delta = 8, 4, 2$, and from the HF approximation (solid and dotted lines) for $U_d = 2\Delta = 2$.

with

$$\Lambda_{\nu,\nu'} = t_{pd}^4 |P(i\nu)| [\tilde{\chi}_{loc}]_{\nu,\nu'} |P(i\nu')|, \quad (36)$$

$$\alpha_{\nu,\nu'} = t_{pd}^4 |P(i\nu)|^2 \delta_{\nu,\nu'}, \quad (37)$$

where, $\tilde{\chi}_{loc}$ is the local paring susceptibility at a d-site given by

$$[\tilde{\chi}_{loc}]_{\nu,\nu'} = T^2 \int_0^\beta d\tau_1 \int_0^\beta d\tau_2 \int_0^\beta d\tau_3 \int_0^\beta d\tau_4 e^{i\nu(\tau_1-\tau_2)} e^{i\nu'(\tau_3-\tau_4)} < T d_\uparrow(\tau_1) d_\downarrow(\tau_2) d_\downarrow^\dagger(\tau_3) d_\uparrow^\dagger(\tau_4) > . \quad (38)$$

To calculate $\tilde{\chi}_{loc}$ within the DMFT-ED method, we use a spectral representation of r.h.s. in eq.(38) by inserting a complete set of eigenstates $|i\rangle$.

When the largest eigen value of Λ, λ_{max}, approaches unity, the paring susceptibility diverges. It signals the transition into the superconducting state from the normal state. In Fig.30, we show the value of λ_{max} as a function of the temperature T for $U_d = 8$ and $\Delta = 4$ at $n = 1.3$ and 1.7 obtained from the DMFT-ED with the system size $N_s = 5$. The value of λ_{max} increases with decreasing T and exceeds unity at a certain critical temperature. For $n = 1.3$, the critical temperature for the spin-singlet pairing, T_{SS}, is higher than that for the spin-triplet pairing, T_{TS}, while, for $n = 1.7$, T_{TS} is higher than T_{SS}[76]. This tendency is consistent with the zero-temperature DMFT-ED result with the system size $N_s = 6 - 8$[58].

We note that the triplet superconductivity is on-site pairing and the gap function is odd in the Matsubara frequency as first proposed by Berezinskii in the superfluid ^{3}He[77]. In the present calculation, the eigen function corresponding to the largest eigen value of Λ for the triplet-pairing, is proportional to the gap function at the critical temperature, and is confirmed to be odd in the Matsubara frequency.

In Fig.31, the superconducting transition temperature for the triplet pairing T_{TS} and that for the singlet pairing T_{SS}, obtained from the DMFT-ED method mentioned above, are plotted as functions of n for $U_d = 8$ and $\Delta = 4$. We also plotted the transition temperature for the ferromagnetism T_c (see Fig. 29) together with that for the antiferromagnetism T_N calculated from the DMFT-ED method with $N_s = 6$. As seen in Fig.31, the singlet superconductivity is realized for $n \lesssim 1.4$ near the antiferromagnetic phase, where the antiferromagnetic fluctuation is considered to be responsible for the singlet pairing. On the other hand, the triplet superconductivity is realized for $T \gtrsim 1.4$ near the ferromagnetic phase, where the ferromagnetic fluctuation is considered to be responsible for the triplet pairing. Significantly, a reentrant superconducting transition is observed for $1.4 \lesssim n \lesssim 1.5$. The reentrant transition has also been observed in the $d = \infty$ periodic Anderson model[78]. Therefore, the

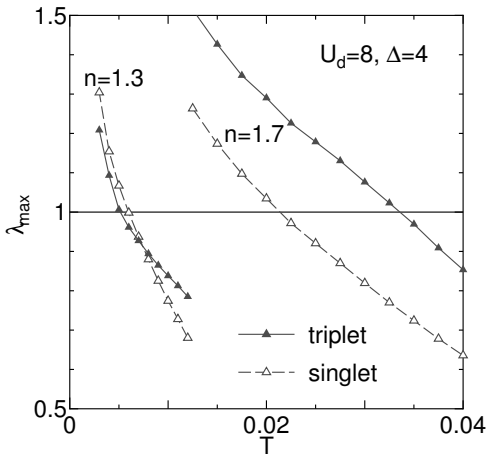

Figure 30: The largest eigen value λ_{max} as a function of the temperature T for $U_d = 8$ and $\Delta = 4$ at $n = 1.3$ and 1.7 obtained from the DMFT-ED with $N_s = 5$.

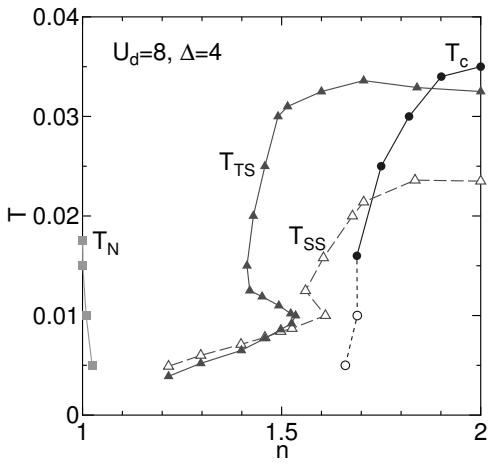

Figure 31: Transition temperatures for the ferromagnetism T_c, the spin-triplet superconductivity T_{TS}, the spin-singlet superconductivity T_{SS} and the antiferromagnetism T_N, obtained from the DMFT-ED for $U_d = 8$ and $\Delta = 4$.

reentrant superconducting transition is considered to be a specific feature of two-band type models including *d-p* model and the periodic Anderson model.

6 Summary and Discussion

We have investigate the ferromagnetism and the related superconductivity of the Hubbard model with two-fold orbital degeneracy and the *d-p* model with paying attention to the effect of the interplay between the Coulomb interactions and the band splitting. To obtain reliable results beyond the perturbative or the mean-field like approximations, we use the numerical diagonalization method for the one-dimensional models and the dynamical mean-field theory for the infinite-dimensional model. For one-dimensional models, we calculate the critical exponent K_ρ based on the Luttinger liquid theory and the paring correlation functions of the ground state.

In the one-dimensional multi-orbital Hubbard model, we have obtained various phase diagrams including the ferromagnetic and the superconducting state on the $U' - J$ parameter plane. The fully polarized ferromagnetism has been found in the strong coupling regime with $U' \gtrsim J \gtrsim \Delta$. For $1 < n < 2$, the ferromagnetism is metallic and mainly caused by the double-exchange mechanism[23]. Crystal-field splitting destroys the fully polarized ferromagnetism resulting in a partially polarized one for $J \lesssim \Delta$. In the vicinity of the partially polarized ferromagnetism, we have found the triplet superconducting phase, when J exceeds the lowest energy of the inter-band excitation. It extends to the realistic parameter region for $3d$ transition-metals with $U' > J$.

Sakamoto *et al.*[23] claimed that the metallic ferromagnetism for $\Delta = 0$ appears in a similar parameter region in any dimension by comparing the results from one dimension with those from infinite dimensions. It is natural to think that this ferromagnetism will appear in two and three dimensions even in the presence of Δ. Then, we expect that a partially polarized (weak) ferromagnetism appears in real materials, in which Hund's rule coupling and crystal-field splitting compete with each other, such as in cobalt oxides. In fact, a weak ferromagnetism has been observed in the layered $Na_{0.75}CoO_2$[13] as well as in the perovskite $R_{1-x}A_xCoO_3$[79]. The orbital degeneracy of $3d$ electrons is considered to play a crucial role in Na_xCoO_2 as well as in $La_{1-x}Sr_xCoO_3$[15].

In our calculation, we can not find any sign of the superconductivity near the fully polarized ferromagnetic state at the realistic parameter region $U' > J$. It suggests that not the complete ferromagnetic state but the weak ferromagnetic state can be a key to the superconductivity of real materials. The competition between Hund's rule coupling and crystal-field splitting causes the large orbital fluctuation, accompanied by the fluctuation between the low-spin and the high-spin states at each Co ion. This fluctuation is expected to mediate the superconductivity near the weak ferromagnetism. Since the orbital fluctuation has a local character, the mechanism for the superconductivity could be common in all dimensions. We therefore think that exploration of the superconductivity in the vicinity of the weak ferromagnetism in the perovskite $R_{1-x}A_xCoO_3$[79] may be promising.

In the one-dimensional *d-p* model, we have calculated the critical exponent K_ρ and the various types of the paring correlation functions. Using the Luttinger liquid relations, we have found that the SC correlation is dominant in the parameter region where the renormalized band becomes almost flat. Since the narrowing of the effective bandwidth leads to the enhancement of the fluctuation, it can cause the superconductivity. The behavior of the paring correlation functions suggests that the singlet paring on a same p site and between the nearest neighbor p sites are most relevant to the superconducting state near half-filling. This result can be interpreted that the antiferromagnetic fluctuation meditates the singlet paring as similar as the t-J model. However, in large doping case $n = 12/7$, the triplet paring between the nearest neighbor p sites becomes relevant to the superconductivity as well as the singlet paring between the nearest neighbor p sites. This result suggests that the low energy physics of the *d-p* model can not well described by the t-J model near $n = 2$. We think that the existence of multi-band might be crucial to understand the triplet paring superconductivity.

We also examine infinite-dimensional *d-p* model based on the dynamical mean-field theory. The dynamical mean-field theory becomes exact in the limit of infinite spatial dimensions and believed to be a good approximation in high dimensions. The result is expected to be complementary to the result of the one-dimensional *d-p* model. We obtain the phase diagrams of the metal-insulator transition on the ground state at half-filling and quarter-filling. We also calculate the magnetization and the pairing susceptibility to obtain the transition temperatures for the ferromagnetism and the superconductivity. It shows that the singlet superconductivity is realized for $n \lesssim 1.4$ near the antiferromagnetic phase, where the antiferromagnetic fluctuation is considered to be responsible for the singlet pairing. On

the other hand, the triplet superconductivity is realized for $T \gtrsim 1.4$ near the ferromagnetic phase. We think that the ferromagnetic fluctuation is responsible for the triplet pairing as well as the one-dimensional case near $n = 2$.

Ferromagnetism and superconductivity has been studied for a long time as a central argument in itinerant electron systems. In this paper, we have presented the electron correlation and the band splitting to be crucial for the ferromagnetism and the related superconductivity in the two types of the two-band Hubbard models. We hope that our work would yield an insight into the deep relationship between these interesting phenomena.

References

[1] For a review, see, for example, Y. Tokura, Ed., *Colossal Magnetoresistive Oxides* (Gordon and Breach Science, New York, 2000).

[2] Y. Maeno, H. Hashimoto, K. Yoshida, S Nishizaki, T. Fujita, J. G. Bednorz and F. Lichtenberg, Nature (London) **372** 532 (1994).

[3] O. Gunnarsson, E. Koch and R. M. Martin, Phys. Rev. **B54** R11026 (1996).

[4] M. Matsukawa, Yuh Yamada, M. Chiba, H. Ogasawara, T. Shibata, A. Matsushita and Y. Takano, Physica C **411** 101 (2004).

[5] G. H. Jonker and J. H. Van Santen, Physica **19** 120 (1953).

[6] R. R. Heikes, R. C. Miller and R. Mazelsky, Physica **30** 1600 (1964).

[7] P. M. Raccah and J. B. Goodenough, Phys. Rev. **155** 932 (1967).

[8] K. Asai, P. Gehring, H. Chou, and G. Shirane, Phys. Rev. **B40** 10982 (1989).

[9] M. Itoh, M. Sugahara, I. Natori and K. Motoya, J. Phys. Soc. Jan. **64** 3967 (1995).

[10] M. Itoh, I. Natori, S. Kubota and K. Motoya, J. Phys. Soc. Jpn. **63** 1486 (1994).

[11] D. Louca, J. L. Sarrao, J. D. Thompson, H. Roder and G. H. Kwei, Phys. Rev. **B60** 10378 (1999).

[12] I. Terasaki, Y. Sasago and K. Uchinokura, Phys. Rev. **B56** R12685 (1997).

[13] T. Motohashi, R. Ueda, E. Naujalis, T. Tojo, I. Terasaki, T. Atake, M. Karppinen and H. Yamauchi, Phys. Rev. **B67** 064406 (2003).

[14] K. Takada, H. Sakurai, E. Takayama-Muromachi, F. Izumi, R. A. Dilanian and T. Sasaki, Nature **422** 53 (2003).

[15] W. Koshibae, K. Tsutsui and S. Maekawa, Phys. Rev. **B62** 6869 (2000).

[16] K. Kusakabe and H. Aoki, Physica. B **194-196** 217 (1994).

[17] W. Gill and D. J. Scalapino, Phys. Rev. **B35** 215 (1987) .

[18] J. Kuei and R. T. Scalettar, Phys. Rev. **B55** 14968 (1997) .

[19] J. E. Hirsch, Phys. Rev. **B56** 11022 (1997).

[20] K. Held and D. Vollhardt, Eur. Phys. J. B **5** 473 (1998).

[21] S. Q. Shen, Phys. Rev. **B57** 6474 (1998).

[22] T. Momoi and K. Kubo, Phys. Rev. **B58** R567 (1998).

[23] H. Sakamoto, T. Momoi and K. Kubo, Phys. Rev. **B65** 224403 (2002).

[24] K. Sano and Y. Ōno, J. M. M. M. **310 (2)** e319 (2007).

[25] H. C. Lee, P. Azaria and E. Boulat, Phys. Rev. **B69** 155109 (2004).

[26] T. Shirakawa, Y. Ohata, S. Nishimoto, J. M. M. M. **310 (2)** 663 (2007)

[27] H. Tasaki, Prog. Theor. Phys. **99** 489 (1998).

[28] J. Sólyom, Adv. Phys. **28**, 201 (1979).

[29] V. J. Emery, in *Highly Conducting One-Dimensional Solids*, edited by J. T. Devreese, R. Evrand and V. van Doren, (Plenum, New York, 1979), p.327.

[30] F.D.M. Haldane, J. Phys. **C14** 2585 (1981).

[31] J. Voit, Rep. Prog. Phys. **58** 977 (1995).

[32] H. J. Schulz, Phys. Rev. Lett. **64** 2831 (1990).

[33] M. Ogata, M. U. Luchini, S. Sorella and F. F. Assaad, Phys. Rev. Lett. **66** 2388 (1991).

[34] K. Sano and Y. Ōno, J. Phys. Soc. Jpn. **63** 1250 (1994);J. Phys. Chem. Solids. **62** 281 (2001); **63** 1567 (2002).

[35] L. Balentz and M.P.A. Fisher, Phys. Rev. **B53** 12133 (1996).

[36] M. Fabrizio, Phys. Rev, B **54** 10054 (1996).

[37] V. J. Emery, S. A. Kivelson and O. Zachar, Phys. Rev. **B59** 15641 (1999).

[38] In this case, the electronic state is described by two-component charge degrees of freedom, while the single band model has a single component charge degree of freedom. The bosonization method for the two-chain model with a small interchain hopping[32, 35, 36, 37] shows that the model has a spin-gaped phase and SC and CDW correlations decay as $\sim r^{-\frac{1}{2K_\rho}}$ and $\sim r^{-2K_\rho}$ respectively (SDW correlations decay exponentially). Hence, SC correlation is dominant for $K_\rho > 0.5$. In this case, one of the charge degree of freedom has a charge gap and the remain has gapless excitations.

[39] K. Sano, Physica **B281&282** 829 (2000); J. Phys. Soc. Jpn. **69** 1000 (2000).

[40] K. Kusakabe, S. Watanabe and Y. Kuramoto, J. Phys. Soc. Jpn. Suppl. **71** 311 (2002).

[41] K. Sano and Y. Ōno, J. Phys. Soc. Jpn. **72** 1847 (2003).

[42] K. Sano and Y. Ōno, J. Phys.: Condens. Matter **19** 14528 (2007).

[43] Detail of the Moebius boundary condition is discussed by T.F.A. Muller and T. M. Rice, Phys. Rev. **B58** 3425 (1998).

[44] R. Assaraf, P. Azaria, M. Caffarel and P. Lecheminant, Phys. Rev. **B60**, 2299 (1999).

[45] M. Imada, J. Phys. Soc. Jpn. **70** 1218 (2001).

[46] K. Yamaji, J. Phys. Soc. Jpn. **70** 1476 (2001).

[47] K. Sano and Y. Ōno, Physica **C205** (1993) 170;Phys. Rev. **B51** (1995) 1175; Physica **C242** 113 (1995).

[48] X. Zotos, W. Lehr and W. Weber, Z. Phys. **B74** 289 (1989).

[49] A. Sudbø, C.M. Varma, T. Giamarchi, E.B. Stechel and T. Scalettar, Phys. Rev. Lett. **70** 978 (1993).

[50] W. Barford and E. R. Gagliano Physica **B194-196**, 1455 (1994); see also, C. Vermeulen, W. Barford and E. R. Gagliano, Europhys. Lett. **28** 653 (1994).

[51] E.B. Stechel, A. Sudbø, T. Giamarchi and C.M. Varma, Phys. Rev. **B51** 553 (1995).

[52] A. W. Sandvik and A. Sudbø, Phys. Rev. **B54** R3746 (1996).

[53] K. Sano and Y. Ōno, J. Phys. Soc. Jpn. **67** 389 (1998);**67** (1998) 4151.

[54] W. Metzner and D. Vollhardt, Phys. Rev. Lett. **62** 324 (1989).

[55] A. Georges, G. Kotliar, W. Krauth and M. J. Rozenberg, Rev. Mod. Phys. **68** 13 (1996).

[56] Th. Pruschke, M. Jarrell and J.K. Freericks, Adv. Phys. **44** 187 (1995).

[57] M. Jarrell, Phys. Rev. Lett. **69** 168 (1992).

[58] M. Caffarel and W. Krauth, Phys. Rev. Lett. **72** 1545 (1994).

[59] O. Sakai and Y. Kuramoto, Solid State Commun. **89** 307 (1994).

[60] R. Bulla, Phys. Rev. Lett. **83** 136 (1999).

[61] J.K. Freericks and M. Jarrell, Phys. Rev. Lett. **74**, 186 (1995).

[62] M. Ulmke, Eur. Phys. J. B **1** 301 (1998).

[63] T. Obermeier, T. Pruschke and J. Keller, Phys. Rev. **B56** R8479 (1997).

[64] M. Jarrell and T. Pruschke, Z. Phys. **B 90**, 187 (1993).

[65] A. Koga, Y. Imai and N. Kawakami, Phys. Rev. **B66** 165107 (2002).

[66] Y. Ōno, M. Potthoff and R. Bulla, Phys. Rev. **B67** 035119 (2003).

[67] A. Georges, G. Kotliar and W. Krauth, Z. Phys. **B 92** 313 (1993).

[68] T. Mutou, H. Takahashi and D. S. Hirashima, J. Phys. Soc. Jpn. **66** 2781 (1997).

[69] Y. Ōno and K. Sano, J. Phys. Chem. Solids **62** 285 (2001).

[70] Y. Ōno, R. Bulla and A. C. Hewson, Eur. Phys. J. B **19** 375 (2001).

[71] Y. Ōno, R. Bulla, A. C. Hewson and M. Potthoff, Eur. Phys. J. B **22** 283 (2001).

[72] Y. Ōno and K. Sano, J. Phys. Soc. Jpn. Suppl. **71** 356 (2002).

[73] Y. Ohashi and Y. Ōno, J. Phys. Soc. Jpn. **70** 2989 (2001).

[74] Y. Ohashi and Y. Ōno, J. Phys. Soc. Jpn. Suppl. **71** 217 (2002).

[75] H. Watanabe and S. Doniach, Phys. Rev. **B57** 3829 (1998).

[76] In our previous paper[69], we reported that T_{SS} is close to T_{TS} and is slightly higher than T_{TS} for all n, but the calculation was done with a smaller system size $N_s = 4$.

[77] V. Berezinskii, JETP Lett. **20** 287 (1974).

[78] A. Tahvildar-Zadeh, M. Hettler and M. Jarrell, Phil. Mag. B **78** 365 (1998).

[79] H. Masuda, T. Fujita, T. Miyashita, M. Soda, Y. Yasui, Y. Kobayashi and M. Sato, J. Phys. Soc. Jpn. **72** 873 (2003).